Hindawi
Mathematical Problems in Engineering
Volume 2021, Article ID 9930017, 21 pages
https://doi.org/10.1155/2021/9930017

Research Article

Impact of Hall Current and Nonlinear Thermal Radiation on Jeffrey Nanofluid Flow in Rotating Frame

Hakeem Ullah,[1] **Abdelaziz Alsubie**,[2] **Mehreen Fiza**,[1] **Nawaf N. Hamadneh**,[2] **Saeed Islam**,[1] **and Ilyas Khan**[3,4]

[1]*Department of Mathematics, Abdul Wali Khan University, Mardan, Pakistan*
[2]*Department of Basic Sciences, College of Science and Theoretical Studies, Saudi Electronic University, Riyadh 11673, Saudi Arabia*
[3]*Department of Mathematics, College of Science Al-Zulfi, Majmaah University, Al-Majmaah 11952, Saudi Arabia*
[4]*Faculty of Mathematics and Statistics, Ton Duc Thang University, Ho Chi Minh City 72915, Vietnam*

Correspondence should be addressed to Ilyas Khan; i.said@mu.edu.sa

Received 10 March 2021; Revised 25 April 2021; Accepted 11 July 2021; Published 31 July 2021

Academic Editor: Ahmad Zeeshan

This research article deals with the nonlinear thermally radiated influences on non-Newtonian nanofluid considering Jeffrey fluid in a rotating system. The governing equations of the nanofluid have been transformed to a set of differential nonlinear equations, using suitable similarity variables. The Homotopy Analysis Method (HAM) and Runge–Kutta Method of order 4 (RK Method of order 4) are used for the solution of the modeled problem. The variation of the skin friction, Nusselt number, Sherwood number, and their impacts on the velocity distribution, temperature distribution, and concentration distribution have been examined. The influence of the Hall effect, rotation, Brownian motion, porosity, and thermophoresis analysis are also investigated. Moreover, for comprehension of the physical presentation of the embedded parameters, Deborah number β, viscosity parameter R, rotation parameter Kr, Brownian motion parameter Nb, porosity parameter γ, magnetic parameter M, Prandtl number Pr, thermophoretic parameter Nt, and Schmidt number Sc have been plotted and deliberated graphically. For large values of Brownian parameter, the kinetic energy increases, which in turn increases the temperature distribution, while the thermal boundary layer thickness decreases by increasing the radiation parameter, and the Hall parameter increases the motion of the fluid in horizontal direction. Also, the mass flux has been observed as a decreasing function at the lower stretching plate.

1. Introduction

The word nanofluid denotes the nanoparticles deferred into the base fluid. Usual examples of nanoparticles contain metals such as copper, aluminum, and silver, nitrides like silicon nitride, carbides such as silicon carbides, oxides like aluminum oxide, and nonmetals such as graphite. The usual liquids are water, oil, and ethylene glycol. The combination of nanoparticles through base liquid enormously develops the thermal qualities of the vile liquid. Choi et al. [1] introduced the term nanofluid and heat transfer features of vile fluids, such as thermal conductivity that is enriched by the addition of nanoparticles into it [2, 3].

Magnetohydrodynamics (MHD) are the information of the magnetic assets of electrically conducting fluids. Plasmas, electrolytes, water, and liquid metals are examples of the such magnetofluids. Hannes Alfven [4] was the first to introduce the field of MHD. Magnetohydrodynamics have several applications in the field of industries and engineering such as plasma, crystal growth, magnetohydrodynamic sensors, liquid-metal cooling of reactors, electromagnetic casting, MHD power generation, and magnetic drug targeting. MHD depends on the strength of the magnetic field; the stronger the magnetic field, the greater the magnetohydrodynamic effects, and vice versa. B.J. Gireesha et al. studied the thermal radiation on MHD boundary layer flow

of Jeffrey nanofluid over stretching sheet [5]. When the magnetic force becomes stronger, then we cannot neglect the Hall effects produced due to the Hall currents. Hall effect is produced due to the potential difference across an electrical conductor when a magnetic field is acting in a direction vertical to that of the flow of current. Edwin Hall [6] was the pioneer to give the concept of Hall current. It is of substantial status and attractive to investigate hydrodynamical problems improved by the influence of Hall currents with their results. Hall currents change flows to cross flow, making it three-dimensional. Pop and Soundalgekar [7] have studied Hall effect on time independent hydromagnetic viscous fluid flow. Ahmed and Zueco [8] have investigated the heat and mass transmission influence to flow in a rotating porous channel by captivating the influence of Hall current and obtained exact solution of the modeled problem. Abdel Aziz [9] has studied Hall effects on the nanofluid flow of viscid flow with heat transmission through a stretching sheet. Hayat [10] has scrutinized the influence of viscous dissipation on mixed convection Jeffrey fluid flow over a vertical stretching surface under the Hall and ion effects. Sulochana [11] has studied unsteady fluid flow over a permeable medium in a rotating parallel plate with Hall effects considering it in three dimensions. Because eccentric features of the nanoliquids make them proficient in many applications, nanofluids are used in the hybrid powered engines, pharmaceutical procedures, fuel cells, and microelectronics, and currently, they are mostly used in the field of nanotechnologies [12]. Wang et al. [13] have given a brief review on nanofluids on the view of their experiments and applications. It enhances the thermal conduction of the base liquid; hence, in the investigation of the flow of nanofluids in a rotating system, the scientists are intensely interested in it. Especially, the flow of nanofluid between parallel plates is one of the standard problems that have significant applications like in accelerators, MHD power generators and pumps, purification of crude oil, aerodynamic heating, petroleum industry, different automobiles sprays, and designing cooling systems with liquid metal. Goodman [14] was the first to study viscous fluid in parallel plates. Borkakoti and Bharali [15] have investigated hydromagnetic viscous flow between parallel plates, where one of them is being a stretching sheet. Attia et al. [16] have examined viscous flow between parallel plates with magnetohydrodynamics. Sheikholeslami et al. [17] have investigated nanofluid flow of viscous fluids between parallel plates with rotating systems in three dimensions under the magnetohydrodynamics (MHD) effects. For the solution of the modeled problems, they used numerical techniques and described the effects of achieving parameters in detail. Mahmoodi and Kandelousi have [18] investigated the hydromagnetic effect of kerosene–alumina nanofluid flow in the occurrence of heat transfer analysis, and differential transformation method is used in their work. Tauseef et al. [19] and Rokni et al. [20] have observed the magnetohydrodynamics and temperature effects on nanofluids flow in parallel plates with rotating system. M. Fiza et al. Studied three-dimensional MHD rotating flow of viscoelastic nanofluid in porous medium between two parallel plates [21]. In the current situation, different hybrid technology is developing day by day. In order to save the energy, the hybrid technology is developed. Fluid flow in a rotating system is a natural phenomenon. In fact, this rotation exists among the fluid particles internally and increases when fluid starts flowing. So, in the natural phenomenon of fluid, flow rotation exists up to some extent. The experimental idea of the viscous fluid motion in a rotating system was given by Taylor and Geoffrey [22]. Greespan [23] has investigated the detailed study of fluid movement in a rotating system. Vajravelua and Kumar [24] have examined magnetohydrodynamics viscous fluid flow amongst binary horizontal and parallel plates in a rotating system, in which one plate is stretched, and the other is permeable. They obtained numerical solution and studied the effect of physical parameters. Their work was extended by Mehmood and Asif [25]. In everyday life's industries and technologies, non-Newtonian fluids are used frequently, and extremely less studies of Newtonian nanofluids to rotating system are found. Hayat et al. [26] have studied non-Newtonian fluid flow with rotation using different models and extended their work in two and three dimensions. Nadeem et al. [27] have investigated micropolar nanofluid in two horizontal and parallel plates with rotation. They obtained the analytical solution of the problem and discussed the embedded parameters. Jena et al. [28] have investigated viscoelastic fluid with the effect of MHD and internal heat in porous channel with rotating system. Jeffrey fluid is the significant subclass of non-Newtonian fluids, which were initially studied by Jeffrey [29]. Shehzad et al. [30] have extended the same work using convective conditions. The detailed study of Jeffery fluid other than the rotating system can be seen in [31–37]. In the field of science and engineering, most of the mathematical problems are complex in their nature, and the exact solution is almost extremely difficult or even not possible. So, for the solution of such problems, numerical and analytical methods are used to find the approximate solution. One of the important and popular techniques for the solution of such type problems is the Homotopy Analysis Method. It is a substitute method, and its main advantage is applying to the nonlinear differential equations without discretization and linearization. Liao [38–40] was the first to investigate this technique for the solution of nonlinear high ordered problems and generally proved that this technique is quickly convergent to the approximated series solutions. Z. shah et al. applied successfully this technique to solve the three-dimensional third-grade nanofluid flow in a rotating system between parallel plates with Brownian motion and thermophoresis effects [41]. Also, this technique provides series solutions in the form of a single variable. Solution by this technique is significant, because it involves all of the physical parameters of a problem, and we can easily discuss its behavior. In all these studies, the impact of Hall current with MHD on Jeffrey fluid has not been studied. So, for this aim, the impact of Hall current with MHD Jeffrey nanofluid with nonlinear thermal radiations in the rotating frame is considered.

2. Problem Formulation

In this section, we describe the physical description and mathematical description of the proposed model.

2.1. Physical Description. The flow of electrically conducting Jeffrey nanofluid between two parallel and horizontal plates is considered. The distance between the upper and lower plates is denoted with h. The coordinate system is selected in such a method that the plate and fluid both are rotated about the y-axis with an angular velocity Ω.. The two forces are assumed to have the same magnitude, but they are opposite in direction, to stretch the lower plate along x-axis, so that the origin $(0, 0, 0)$ remains constant. The flow of the fluid and temperature transfer is considered in steady state, which is incompressible, laminar, and stable. The surface temperature of the nanofluid between parallel plates is taken after the influence of convective heating process, and its temperature of the hot fluid is T_0 under the surface. The free stream is occupied at a uniform ambient nanofluid temperature T_h with $T_0 > T_h$. A magnetic field B_0 is acting in y direction, with which the system is rotating. In addition, the effect of Hall current is taken in the nanofluid model. Here, the fluids are electrically conducting, and when the magnetic field becomes stronger, the Hall current is produced, which affects the nanofluids. This effect gives increase to a force in z−direction, which tempts a cross flow in the same direction, and hence, the nanofluid flows in a deflected way into three dimensions, as shown in Figure 1.

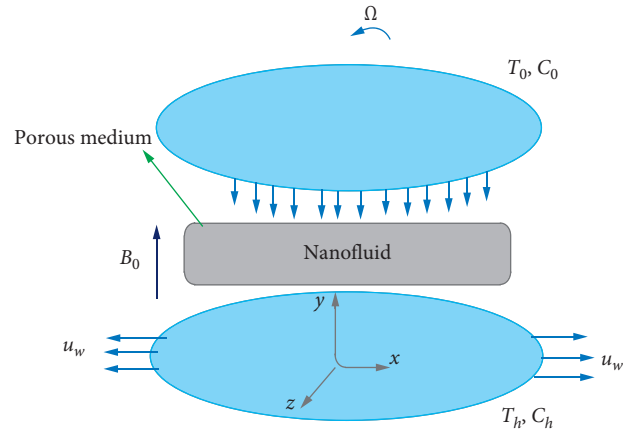

Figure 1: Physical model of the nanofluid flow problem.

2.2. Mathematical Description. Ohm's law in generalized form containing the Hall current is written as [3–7]

$$J + \frac{\omega_e t_e}{B_0} \times (J \times B) - \sigma_{nf}(E + V \times B) - \frac{\sigma_{nf} P_e}{e n_e} = 0. \tag{1}$$

Here, $J = (J_x, J_y, J_z)$ represents the current density, $B = (0, B_0, 0)$ represents the magnetic field, E represents the intensity of electric field, $V = (u, v, w)$ represents the velocity components, ω_e represents the oscillating frequency of the electron, t_e denotes the time of electron collision, σ_{nf} denotes the electrical conductivity, e is the charge of electron, n_e is the number density of electron, and P_e is the pressure of the electron. We take $E = 0$, because the applied voltage imposed on the flow of nanofluid is zero. In case of weak ionized molecules, the Law of Ohm in a generalized form in the view of the aforementioned circumstances provides $(J_y = 0)$ in the flow field. Using these assumptions, we get J_x and J_y as

$$J_{x.} = \frac{\sigma_{nf} B_0^2}{1 + m^2}(mu - w), \tag{2}$$

$$J_z = \frac{\sigma_{nf} B_0^2}{1 + m^2}(u + mw). \tag{3}$$

Here, $m = \omega_e t_e$ is the Hall parameter. The rheological model that illustrates the Jeffrey fluids is known as [24–34]

$$\mathbf{S} = \frac{\mu}{\lambda_1}\left(\mathbf{L} + \lambda_2 \frac{D\mathbf{L}}{Dt}\right). \tag{4}$$

$\mathbf{S}$ denotes Cauchy stress tensor, μ denotes the dynamic viscosity of the Jeffrey fluid $\mathbf{L} = \nabla \mathbf{v} + (\nabla \mathbf{v})^T$, and λ_1 and λ_2 are a ratio of relaxation and retardation time respectively. Observance in light of the above deliberation, the elementary equations of continuity, velocity, energy, and concentration are articulated as

$$\frac{\partial u}{\partial x} + \frac{\partial v}{\partial y} + \frac{\partial w}{\partial z} = 0, \tag{5}$$

$$\begin{aligned} \rho_f\left(u\frac{\partial u}{\partial x} + v\frac{\partial u}{\partial y} + 2w\Omega\right) &= -\frac{\partial P}{\partial x} + \frac{\mu}{1+\lambda_1}\left(\frac{\partial^2 v}{\partial x^2} + \frac{\partial^2 v}{\partial y^2}\right) - \frac{\sigma B_0^2}{1+m^2}(u + mw) + \frac{\mu\gamma_2}{1+\lambda_1} - \frac{\nu}{\kappa}u \\ &\cdot\left[\left(2\frac{\partial u}{\partial x}\frac{\partial^2 u}{\partial x^2} + 2\frac{\partial v}{\partial x}\frac{\partial^2 u}{\partial x\,\partial y}\right) + u\left(\frac{\partial^3 u}{\partial x^3} + \frac{\partial^3 u}{\partial x\,\partial y^2}\right) + v\left(\frac{\partial^3 u}{\partial x^2 \partial y} + \frac{\partial^3 u}{\partial y^3}\right)\right. \\ &\left. + \frac{\partial u}{\partial y}\left(\frac{\partial^2 v}{\partial x^2} + \frac{\partial^2 u}{\partial y\,\partial x}\right) + \left(\frac{\partial^2 u}{\partial y^2} + \frac{\partial^2 v}{\partial x\,\partial y}\right)\frac{\partial v}{\partial y}\right], \end{aligned} \tag{6}$$

$$\rho_f\left(u\frac{\partial v}{\partial x}+v\frac{\partial v}{\partial y}\right)=-\frac{\partial P}{\partial y}+\frac{\mu}{1+\gamma_1}\left(\frac{\partial^2 v}{\partial x^2}+\frac{\partial^2 v}{\partial y^2}\right)+\frac{\mu\gamma_2}{1+\gamma_1}\cdot\left[\left(2\frac{\partial v}{\partial y}\frac{\partial^2 v}{\partial y^2}+2\frac{\partial u}{\partial y}\frac{\partial^2 v}{\partial y\,\partial x}\right)+\left(\frac{\partial^3 v}{\partial x^3}+\frac{\partial^3 v}{\partial x\,\partial y^2}\right)u+\left(\frac{\partial^3 v}{\partial x^2\partial y}+\frac{\partial^3 v}{\partial\partial y^2}\right)v+\left(\frac{\partial^2 u}{\partial x\,\partial y}+\frac{\partial^2 v}{\partial x^2}\right)\frac{\partial u}{\partial x}+\left(\frac{\partial^2 u}{\partial y^2}+\frac{\partial^2 v}{\partial x\,\partial y}\right)\frac{\partial v}{\partial x}\right],\tag{7}$$

$$\rho_f\left(u\frac{\partial \omega}{\partial y}+v\frac{\partial \omega}{\partial y}-2\Omega u\right)=\frac{\mu}{1+\lambda_1}\left(\frac{\partial^2 \omega}{\partial x^2}+\frac{\partial^2 \omega}{\partial y^2}\right)-\frac{\sigma_{nf}B_0^2}{1+m^2}(mu-w)+\frac{\mu\gamma_2}{1+\lambda_1}-\frac{\nu}{\kappa}w\cdot\left[\left(\frac{\partial^2 \omega}{\partial y^2}+\frac{\partial^2 \omega}{\partial x\,\partial y}\right)\frac{\partial v}{\partial y}+\left(u\frac{\partial^3 \omega}{\partial y^3}+v\frac{\partial^3 \omega}{\partial x^2\partial y}\right)v+\frac{\partial^2 \omega}{\partial x\,\partial y}\frac{\partial u}{\partial y}+\frac{\partial u}{\partial x}\frac{\partial^2 \omega}{\partial x^2}+\left(\frac{\partial^3 \omega}{\partial x^3}+\frac{\partial^3 \omega}{\partial x\,\partial y^2}\right)\right],\tag{8}$$

$$u\frac{\partial T}{\partial x}+v\frac{\partial T}{\partial y}+w\frac{\partial T}{\partial z}=\alpha\left(\frac{\partial^2 T}{\partial x^2}+\frac{\partial^2 T}{\partial y^2}+\frac{\partial^2 T}{\partial z^2}\right)-\frac{1}{(\rho c)_f}\frac{\partial q_r}{\partial y}-\frac{Q_0}{(\rho c)_f}(T-T_0)+\tau\left[D_B\left\{\frac{\partial C}{\partial x}\frac{\partial T}{\partial x}+\frac{\partial C}{\partial y}\frac{\partial T}{\partial y}+\frac{\partial C}{\partial z}\frac{\partial T}{\partial z}\right\}+\left(\frac{D_T}{T_C}\right)\left\{\left(\frac{\partial T}{\partial x}\right)^2+\left(\frac{\partial T}{\partial y}\right)^2+\left(\frac{\partial T}{\partial z}\right)^2\right\}\right],\tag{9}$$

$$u\frac{\partial C}{\partial x}+v\frac{\partial C}{\partial y}+w\frac{\partial C}{\partial z}=D_B\left(\frac{\partial^2 C}{\partial x^2}+\frac{\partial^2 C}{\partial y^2}+\frac{\partial^2 C}{\partial z^2}\right)+\frac{D_T}{T_0}\left\{\frac{\partial^2 T}{\partial x^2}+\frac{\partial^2 T}{\partial y^2}+\frac{\partial^2 T}{\partial z^2}\right\}.\tag{10}$$

Here, u, v and w symbolize the components of the velocity along x, y and z directions. In equations (2)–(10), the symbols υ, μ represent the coefficient of kinematic and dynamic viscosities, respectively, ρ is density, σ denotes electrical conductivity, and Ω is the angular velocity. In equation (9), T represents temperature, α is the thermal diffusivity, c_p represents specific heat, thermal conductivity of fluid is represented by k, the coefficient of Brownian diffusion is denoted by D_B, and the thermophoretic diffusion coefficient is denoted by D_T. The $\tau = ((\rho c)_p/(\rho c)_f)$ is defined as nanoparticles and effective heat capacity ratio, ρ_f denotes the base fluid density, ρ_b represents density of the particles, and C is coefficient concentration of the fluids particles. q_r indicates the radioactive heat fluctuation, which is given by Rosseland approximation as

$$q_r=-\frac{16\varphi}{3K}\frac{\partial T^4}{\partial y},\tag{11}$$

where φ denoted the Stefan Boltzmann constant and K denoted the mean absorption coefficient. Using Taylor Series, equation, we get

$$T^4=T_0^4+4T_0^3(T-T_0)^2+\cdots.\tag{12}$$

By neglecting higher-order term, we get

$$T^4=4TT_0^3-3T_0^4.\tag{13}$$

Inserting equations (13) into (11), it is reduced to the form

$$\frac{\partial q_r}{\partial y}=-\frac{16T_C^3\varphi}{3K}\frac{\partial^2 T}{\partial y^2}.\tag{14}$$

For state problem, the boundary conditions are defined as

$$\begin{aligned}&u=ax,\\&v=0,\\&w=0,\\&T=T_h,\\&C=C_d,\quad \text{when } y=0,\\&u=v=0,\\&w=0,\\&T=T_0,\\&C=C_0,\quad \text{when } y=h.\end{aligned}\tag{15}$$

The nondimensional variables are presented as

$$\begin{aligned}u&=\alpha x f'(\eta),\\v&=-\alpha h f(\eta),\\w&=\alpha x g(\eta),\\\Theta(\eta)&=\frac{T-T_h}{T_0-T_h},\\\Phi(\eta)&=\frac{C-C_h}{C_0-C_h},\end{aligned}\tag{16}$$

where $\eta = (y/h)$.

Substituting the nondimensional variables from the equations (16) in (1)–(10), equation (1) holds identically, and

the other governing equations are reduced to the following form:

$$f^{iv} + (1+\lambda_1)\left(R\left(ff''' - f'f''\right) - 2\mathrm{Kr}g' - \frac{M}{1+m^2}\left(f'' + mg'\right) - \gamma f''\right) + \beta\left(2f''f''' - ff^{iv} - f'f^{v}\right) = 0, \tag{17}$$

$$g'' + (1+\lambda_1)\left(R\left(fg' - gf'\right) + 2\mathrm{Kr}f' + \frac{M}{1+m^2}\left(mf' - g\right) - \gamma g\right) + \beta\left(g'f'' - fg'''\right) = 0, \tag{18}$$

$$\frac{\mathrm{d}}{\mathrm{d}\eta}\left(1 + \frac{4}{3}\mathrm{Rd}\left(\Theta_f + \left(\Theta_f - 1\right)\right)\Theta\right)\Theta' + \mathrm{Pr}\left(\mathrm{Re}f\Theta' + \mathrm{Nb}\Phi'\Theta' + \mathrm{Nt}\left(\Theta'\right)^2\right) + \lambda\theta = 0, \tag{19}$$

$$\Phi'' + \mathrm{ReSc}f\Phi' + \frac{\mathrm{Nt}}{\mathrm{Nb}}\Theta'' = 0. \tag{20}$$

Using of equation (16) in (15), it reduced the boundary conditions in the form

$$\begin{aligned} f &= 0,\\ f' &= 1,\\ g &= 0,\\ \theta &= 1,\\ \phi &= 1,\\ \eta &= 0,\\ f &= 0,\\ f' &= 0,\\ g &= 0,\\ \theta &= 0,\\ \phi &= 0,\\ \eta &= 1. \end{aligned} \tag{21}$$

The nondimensional physical parameters after generalization are

$$\begin{aligned} \mathrm{Kr} &= \frac{2\Omega h^2}{\nu},\\ \mathrm{Re} &= \frac{ah^2}{\nu},\\ \gamma &= \left(\frac{h^2}{\rho\kappa}\right),\\ M &= \frac{\sigma B_0^2 h^2}{\rho\upsilon},\\ \mathrm{Pr} &= \frac{\mu}{\rho_f \alpha},\\ \beta &= \lambda_2\alpha,\\ \mathrm{Nb} &= \frac{(\rho c)_p D_B C_h}{\alpha(\rho c)_f},\\ \mathrm{Nt} &= \frac{(\rho c)_p D_T T_0}{(\rho c)_f T_c},\\ \mathrm{Rd} &= \frac{4T_c^3\varphi}{k\mathrm{K}},\\ \mathrm{Sc} &= \frac{\mu}{D\rho_f}, \end{aligned} \tag{22}$$

where Kr denotes rotation parameter, M is the magnetic parameter, Re is the viscosity parameter, γ is the porosity parameter, β is the Deborah number, Pr is P and tl number, Sc denotes the Schmidt number, Nb is the parameter of Brownian, Rd is the radiation parameter, and Nt is the thermophoretic parameter.

The Skin friction is defined as

$$C_f = \frac{\left(S_{xy}\right)_{y=0}}{\rho U_w^2}, \tag{23}$$

where

$$C_f = \frac{\left(\mu/(1+\lambda_1)\right)\left[\left(\partial^2 v/\partial x^2\right) + \left(\partial^2 v/\partial y^2\right) + \lambda_2\left(u\left(\partial^2 u/\partial x\,\partial y\right) + v\left(\partial^2 v/\partial x\,\partial y\right) + u\left(\partial^2 v/\partial x^2\right) + v\left(\partial^2 u/\partial y^2\right)\right)\right]_{y=0}}{\rho U_w^2},$$

$$C_f\sqrt{\mathrm{Re}_x} = \frac{1}{1+\lambda_1}\left(f''(0) + \beta f''(0)\right), \tag{24}$$

where R_{ex} is called local Reynolds number defined as $R_{ex} = (U_w x/\nu)$. The Nusselt number is defined as $\mathrm{Nu} = (hQ_w/\widehat{k}(T_0 - T_h))$. Q_w is the heat flux and $Q_w = -\widehat{k}(\partial T/\partial y)_{y=0}$. The Sherwood number is defined as $\mathrm{Sh} = (hJ_w/D_B(C_0 - C_h))$, J_w is the mass flux, and $J_w = -D_B(\partial C/\partial y)_{y=0}$. Here, the dimensionless forms of Nu and Sh are obtained as

$$\begin{aligned} \mathrm{Nu} &= -\left(1 + \frac{4}{3}\mathrm{Rd}\left(\Theta_f + \left(\Theta_f - 1\right)\right)\Theta\right)\Theta'(0), \\ \mathrm{Sh} &= -\Phi'(0). \end{aligned} \tag{25}$$

3. Solution by HAM

Liao was the first one who proposed the Homotopy analysis method (HAM). He deduced HAM from one of the fundamental ideas of the topology called Homotopy. He used two Homotopic functions in the derivation of this technique. The functions are called Homotopic functions when one of them can be continuously distorted into another. Consider that f_1, f_2 are two functions that are continuous, and X, Y are two topological spaces, where f_1 and f_2 map from X to Y, and then f_1 is said to be homotopic to f_2 if they produce continuous function $\widehat{F}$

$$\widehat{F}\colon X \times [0,1] \longrightarrow Y. \tag{26}$$

such that $\forall, x \in \mathrm{X}$

$$\widehat{F}[x,0] = f_1(x)\ \&\ \widehat{F}[x,1] = f_2(x). \tag{27}$$

Then, this mapping $\widehat{F}$ is called Homotopic. Ham is a substitute method, and it is mainly applied to the nonlinear differential equations without discretization and linearization. This technique has several advantages; some of them are as follows: (i) it is free from the values of the parameters, which may be small or large. (ii) It assures the convergence of the solution. (iii) It is self-determining for an assortment of base function and linear operator.

The solutions of equations (17)–(20) with the consistent boundary conditions (21) are obtained by the use of analytic technique. Solution results obtained by HAM contained the assisting parameters h, which adjust and control to converge the solutions and bases functions. The initial guesses are

$$\begin{aligned} f_0(\eta) &= \eta - 2\eta^2 + \eta^3, \\ g_0(\eta) &= 0, \\ \Theta_0(\eta) &= 1 - \eta, \\ \Phi_0(\eta) &= 1 - \eta. \end{aligned} \tag{28}$$

The linear operators are selected in the following way:

$$\begin{aligned} L_f(f) &= f_{\eta\eta\eta\eta}, \\ L_g(g) &= g_{\eta\eta}, \\ L_\Theta(\Theta) &= \Theta_{\eta\eta}, \\ L_\Phi(\Phi) &= \Phi_{\eta\eta}. \end{aligned} \tag{29}$$

The above-mentioned differential operators contents are shown as follows:

$$\begin{aligned} L_f\left(\kappa_1 + \kappa_2\eta + \kappa_3\eta^2 + \kappa_4\eta^3\right) &= 0, \\ L_g\left(\kappa_5 + \kappa_6\eta\right) &= 0, \\ L_\Theta\left(\kappa_7 + \kappa_8\eta\right) &= 0, \\ L_\Phi\left(\kappa_9 + \kappa_{10}\eta\right) &= 0. \end{aligned} \tag{30}$$

Here, $\sum_{m=1}^{10}\kappa_m$ where $m = 1, 2, 3, \ldots$ are arbitrary constants.

3.1. Zeroth-Order Deformation Problem. Expressing $\mathrm{P} \in [\,0\ \ 1\,]$ as an embedding parameter with associate parameters $\hbar_f, \hbar_g, \hbar_\theta$ and $\hbar_\phi$ where $\hbar \neq 0$, then, the problem in case of zero order deforms to the following form:

$$\begin{aligned} (1-P)L_f\left(\widehat{f}(\eta,P) - f_0(P)\right) &= P\hbar_f N_f(\widehat{f}(\eta,P), \widehat{g}(\eta,P)), \\ (1-P)L_g\left(\widehat{g}(\eta,P) - g_0(\eta)\right) &= P\hbar_g N_g(\widehat{f}(\eta,P), \widehat{g}(\eta,P)), \\ (1-P)L_\Theta\left(\widehat{\Theta}(\eta,P) - \Theta_0(\eta)\right) &= P\hbar_\Theta N_\Theta(\widehat{f}(\eta,P), \widehat{g}(\eta,P), \widehat{\Theta}(\eta,P)), \\ (1-P)L_\Phi\left(\widehat{\Phi}(\eta,P) - \Phi_0(\eta)\right) &= P\hbar_\Phi N_\Phi(\widehat{f}(\eta,P), \widehat{\Theta}(\eta,P), \widehat{\Phi}(\eta,P)). \end{aligned} \tag{31}$$

The boundary conditions in homotopic form are written as

$$\begin{aligned} \widehat{f}(0,P) = \widehat{f}'(0,P) = \widehat{g}(0,P) = \widehat{\Theta}(0,P) = \widehat{\Phi}(0,P) = 0, \\ \widehat{f}(1,P) = \widehat{f}'(1,P) = \widehat{g}(1,P) = \widehat{\Theta}(1,P) = \widehat{\Phi}(1,P) = 0. \end{aligned} \tag{32}$$

The resultant nonlinear operators are

$$\begin{aligned} N_f(\widehat{f}(\eta;P), \widehat{g}(\eta;P)) = {} & \widehat{f}_{\eta\eta\eta\eta}(\eta;P)(1+\lambda_1)\left(\frac{M}{1+m^2}\left(\widehat{f}_{\eta\eta}(\eta;P) + m\widehat{g}_\eta(\eta;P)\right) - \gamma\widehat{f}_{\eta\eta}(\eta;P)\right) \\ & + (1+\lambda_1)\left(R\left(\widehat{f}(\eta;P)\widehat{f}_{\eta\eta\eta}(\eta;P) - \widehat{f}_\eta(\eta;P)\widehat{f}_{\eta\eta}(\eta;P)\right) - 2\mathrm{Kr}\widehat{g}_\eta(\eta;P)\right) \\ & + \beta\left(2\widehat{f}_{\eta\eta}(\eta;P)\widehat{f}_{\eta\eta\eta}(\eta;P) - \widehat{f}(\eta;P)\widehat{f}_{\eta\eta\eta\eta}(\eta;P) - \widehat{f}_\eta(\eta;P)\widehat{f}_{\eta\eta\eta\eta}(\eta;P)\right), \end{aligned}$$

$$
\begin{aligned}
N_g(\widehat{g}(\eta;P),\widehat{f}(\eta;P)) &= \widehat{g}_{\eta\eta}(\eta;P) - (1+\lambda_1)\frac{M}{1+m^2}\left(m\widehat{f}_\eta(\eta;P) - \widehat{g}(\eta;P)\right) - \gamma\widehat{g}(\eta;P)\\
&\quad + (1+\lambda_1)\Big(R\Big(\widehat{f}(\eta;P)\widehat{g}_\eta(\eta;P) - \widehat{g}(\eta;P)\widehat{f}_\eta(\eta;P)\Big) + 2\mathrm{Kr}\widehat{f}_\eta(\eta;P)\Big)\\
&\quad + \beta\Big(\widehat{g}_\eta(\eta;P)\widehat{f}_{\eta\eta}(\eta;P) - \widehat{f}(\eta;P)\widehat{g}_{\eta\eta\eta}(\eta;P)\Big),\\
N_\Theta(\widehat{\Theta}(\eta;P),\widehat{f}(\eta;P),\widehat{\Phi}(\eta;P)) &= \frac{\mathrm{d}}{\mathrm{d}\eta}\left[\left(1+\frac{4}{3}\mathrm{Rd}\Big(\Theta_f + \big(\Theta_f - 1\big)\Big)\Theta\right)\widehat{\Theta}_\eta(\eta;P)\right]\\
&\quad + \mathrm{Pr}\Big(R\widehat{f}(\eta;P)\widehat{\Theta}_\eta(\eta;P) + \mathrm{Nb}\widehat{\Phi}_\eta(\eta;P)\widehat{\Theta}_\eta(\eta;P) + \mathrm{Nt}\big(\widehat{\Theta}_\eta(\eta;P)\big)^2\Big),\\
N_\Phi(\widehat{f}(\eta;P),\widehat{g}(\eta;P),\widehat{\Theta}(\eta;P),\widehat{\Phi}(\eta;P)) &= \widehat{\Phi}_{\eta\eta}(\eta;P) + R\mathrm{Sc}\widehat{f}_\eta(\eta;P)\widehat{\Phi}_\eta(\eta;P)\\
&\quad + \frac{\mathrm{Nt}}{\mathrm{Nb}}\widehat{\Theta}_{\eta\eta}(\eta;P).
\end{aligned}
\tag{33}
$$

Using Taylor's series expansion to expand $\widehat{f}(\eta;P), \widehat{g}(\eta;P), \widehat{\Theta}(\eta;P)$ and $\widehat{\Phi}(\eta;P)$ in termd of P, we get

$$
\begin{aligned}
\widehat{f}(\eta,P) &= f_0(\eta) + \sum_{i=1}^{\infty} f_i(\eta),\\
\widehat{g}(\eta,P) &= g_0(\eta) + \sum_{i=1}^{\infty} g_i(\eta),\\
\widehat{\Theta}(\eta,P) &= \Theta_0(\eta) + \sum_{i=1}^{\infty} \Theta_i(\eta),\\
\widehat{\Phi}(\eta,P) &= \Phi_0(\eta) + \sum_{i=1}^{\infty} \Phi_i(\eta),
\end{aligned}
\tag{34}
$$

where

$$
\begin{aligned}
f_i(\eta) &= \frac{1}{i!}\widehat{f}_\eta(\eta,P)|_{P=0},\\
g_i(\eta) &= \frac{1}{i!}\widehat{g}_\eta(\eta,P)|_{P=0},\\
\Theta_i(\eta) &= \frac{1}{i!}\widehat{\Theta}_\eta(\eta,P)|_{P=0},\\
\Phi_i(\eta) &= \frac{1}{i!}\widehat{\Phi}_\eta(\eta,P)|_{P=0}.
\end{aligned}
\tag{35}
$$

3.2. ith-Order Deformation Problem. Differentiating zeroth-order equation i th time, we obtained the i th order deformation equations with respect to P, dividing by $i!$ and then inserting $P = 0$. So, i^{th} order deformation equations are as follows:

$$
\begin{aligned}
L_f\left(f_i(\eta) - \xi_i f_{i-1}(\eta)\right) &= h_f\mathfrak{R}_i^f(\eta),\\
L_g\left(g_i(\eta) - \xi_i g_{i-1}(\eta)\right) &= h_g\mathfrak{R}_i^g(\eta),\\
L_\Theta\left(\Theta_i(\eta) - \xi_i\Theta_{i-1}(\eta)\right) &= h_\Theta\mathfrak{R}_i^\Theta(\eta),\\
L_\Phi\left(\Phi_i(\eta) - \xi_i\Phi_{i-1}(\eta)\right) &= h_\Phi\mathfrak{R}_i^\Phi(\eta).
\end{aligned}
\tag{36}
$$

The resultant boundary conditions are

$$
\begin{aligned}
&\widehat{f}_i = \widehat{f}'_i = \widehat{g}_i = \widehat{\Theta}_i = \widehat{\Phi}_i = 0, \quad \text{at } \eta = 0,\\
&\widehat{f}_i = \widehat{f}' = \widehat{g}_i = \widehat{\Theta}_i = \widehat{\Phi}_i = 0, \quad \text{at } \eta = 1,\\
&\mathfrak{R}_i^f(\eta) = f_{i-1}^{iv} + 2\mathrm{Kr}g_{i-1} + (1+\lambda_1)\\
&\qquad \cdot\left[R\sum_{j=0}^{i-1}\left(f_{i-1-j}f_j'' - f_{i-1-j}'f_j''\right)\right.\\
&\qquad \left. - \frac{M}{1+m^2}\left(f_{i-1}'' + mg_{i-1}'\right) - \gamma f_{i-1}''\right]\\
&\qquad + \beta\sum_{j=0}^{i-1}\left(2f_{i-1-j}''f_j'' - f_{i-1-j}f_j^{iv}f - f_{i-1-j}'f_j^{v}\right),\\
&\mathfrak{R}_i^g(\eta) = g_{i-1}'' - (1+\lambda_1)R\sum_{j=0}^{k-1}\left(f_{i-1-j}g_j' - g_{i-1-j}f_j'\right) + \mathrm{Kr}f_{i-1}'\\
&\qquad - \frac{M}{1+m^2}\left(mf_{i-1}' - g_{i-1}\right) - \gamma g_{i-1}\\
&\qquad + \beta\left(\sum_{j=0}^{i-1} g_{i-1-j}'f_j'' - f_{i-1-j}g_j''\right),\\
&\mathfrak{R}_i^\Theta(\eta) = \frac{\mathrm{d}}{\mathrm{d}\eta}\left[\left(1+\frac{4}{3}\mathrm{Rd}\Big(\Theta_f + \big(\Theta_f - 1\big)\Big)\Theta\right)\Theta_{i-1}'\right]\\
&\qquad + \mathrm{Pr}\left[\mathrm{Re}\sum_{j=0}^{i-1} f_{i-1-j}\Theta_j' + \mathrm{Nb}\sum_{j=0}^{i-1}\Phi_{i-1-j}'\Theta_j\right.\\
&\qquad \left. + \mathrm{Nt}\sum_{j=0}^{i-1}\Theta_{i-1-j}''\Theta_j'\right],\\
&\mathfrak{R}_i^\Phi(\eta) = \Phi_{i-1}'' + R\mathrm{Sc}\sum_{j=0}^{i-1} f_{i-1-j}\Phi_j' + \frac{\mathrm{Nt}}{\mathrm{Nb}}\Theta_{i-1}'',
\end{aligned}
\tag{37}
$$

where

$$\xi_i = \left\{ \begin{array}{l} 1, \ \text{if } P > 1, \\ 0, \ \text{if } P \le 1. \end{array} \right\} \tag{38}$$

The overall homotopic solutions $(f_i, g_i, \Theta_i, \Phi_i)$ of equation (27) in terms of special solutions $(\widehat{f}_i, \widehat{g}_i, \widehat{\Theta}_i, \widehat{\Phi}_i)$ are specified as

$$\begin{aligned} f_i(\eta) &= \widehat{f}_i(\eta) + \kappa_1 + \kappa_2\eta + \kappa_3\eta^2 + \kappa_4\eta^3, \\ g_i(\eta) &= \widehat{g}_i(\eta) + \kappa_5 + \kappa_6\eta, \\ \Theta_i(\eta) &= \widehat{\Theta}_i(\eta) + \kappa_7 + \kappa_8\eta, \\ \Phi_i(\eta) &= \widehat{\Theta}_i(\eta) + \kappa_9 + \kappa_{10}\eta. \end{aligned} \tag{39}$$

4. Convergence of HAM Solution

When we compute the series solutions of the velocity, temperature, and concentration functions to use HAM, the assisting parameters $\hbar_f, \hbar_g, \hbar_\Theta$ and $\hbar_\Phi$ appear. These assisting parameters are responsible for adjusting the convergence of these solutions. In the possible region of $\hbar$, $\hbar$-curves of $f'''(0), g'(0), \Theta'(0)$ and $\Phi'(0)$ for 12^{th} order approximation are plotted in Figures 2 and 3 for different values of embedding parameter. The $\hbar$-curves consecutively display the valid region. Table 1 displays the numerical values of HAM solutions at different approximations using dissimilar values of parameters. It is clear from the table that homotopy analysis technique is a speedily convergent technique. The region of convergence for the velocity distribution $f(\eta)$ and $g(\eta)$ is given as $-3 \le \hbar \le 1$ and $-3.8 \le \hbar \le 1.7$, respectively, while, for the temperature and concentration profile, the convergence regions are given as $-2.6 \le \hbar \le 0.5$ and $-2.1 \le \hbar \le 0.4$, respectively.

5. Results and Discussion

5.1. Graphical Discussion. The present investigation has been carried out to study the flow of non-Newtonian nanofluid (considering the Jeffrey fluid) in a rotating system under the influence of MHD between parallel plates. In addition, the effect of Hall current is given, where the medium between the plates is kept porous. The main aim of this subsection is to study the physical effects of different embedding parameters on the velocity distributions $f(\eta), g(\eta)$, temperature distribution $\Theta(\eta)$, and concentration distribution $\Phi(\eta)$, which are illustrated in Figures (4)–(18). The influence of viscosity parameter Re on the velocity distributions $f(\eta)$ and $g(\eta)$ is shown in Figures 4(a) and 4(b). It is clear that increasing the viscosity parameter Re decreases the velocity distributions $f(\eta)$ and $g(\eta)$. The larger values of Re reduce the viscous forces, which generate the stronger inertial forces, and as a consequence, the velocity field retarded. The strong inertial forces resist the flow, and as a result, the velocity distribution recues. Figure 5(a) displays the effect of viscosity parameter Re on the temperature distribution $\Theta(\eta)$, and the same effect of temperature distribution has been observed, because the larger values of viscosity parameter Re strengthen the inertial forces and tend to reduce

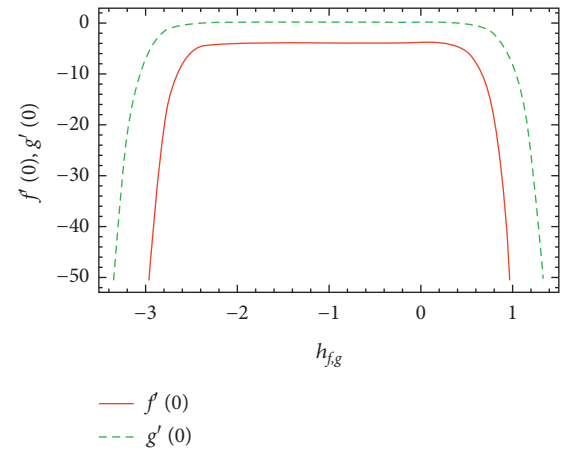

Figure 2: Combined h curves of functions velocity $f(\eta)$ and $g(\eta)$ profiles at 12^{th} order approximation.

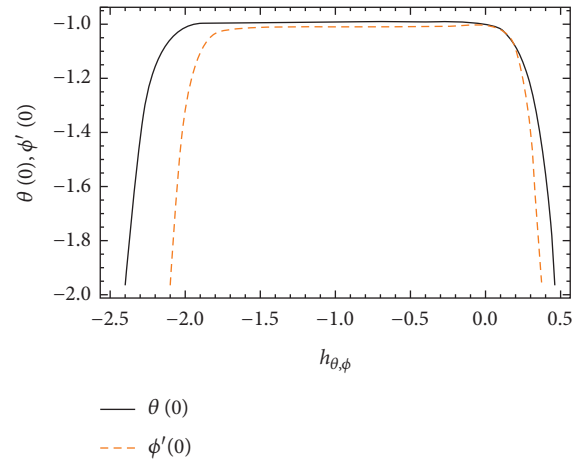

Figure 3: Combined h curves of temperature and concentration $\Theta(\eta)$ and $\Phi(\eta)$ profiles at 12^{th} order approximation.

the temperature field. Figure 5(b) shows the effect of Re on the concentration distribution $\Phi(\eta)$. The rise in Re increases the concentration distribution $\Phi(\eta)$. It means that the thermal conductivity contributed to improve the heat transfer. Also, these observations have been found to be the same as what has been discussed in Sheikholeslami et al. [17], Mahmoodi et al. [18], and Jena et al. [20]. The influence of Kr on the velocity profiles has been shown in Figures 6(a), and 6(b). It is ostensible that when a rotation parameter Kr increases, it raises the fluid motion, and this effect is clearer at the stretching plate, because the rise in rotation parameter Kr increases the Coriolis force, which results in a rise in rotational velocity. An increase in rotation parameter of the fluid increases the kinetic energy of the fluid particles, which in turn increases the flow motion. The effect of Hall parameter m on the velocity profiles $f(\eta)$ and $g(\eta)$ is shown in Figures 7(a) and 7(b). The Hall effect is the production of potential difference. Here, the Hall parameter m plays an important role in the nanofluid flow. The large value of Hall parameter m reduces the effective conductivity, which drops the magnetic damping force, and so, the velocity profile

Table 1: The convergence of HAM up to 20th order approximations when $\mathrm{Rd} = 0.5, \mathrm{Re} = \mathrm{Nt} = \mathrm{Nb} = \beta = \mathrm{Sc} = \mathrm{Pr} = \lambda_1 = M = m = M = 0.01, \gamma = 0.1$.

Order of approximation	$f''(0)$	$g'(0)$	$\Theta'(0)$	$\Phi'(0)$
1	3.98886	−0.0207921	0.953750	1.00025
4	3.97650	−0.0387064	0.913169	1.07375
8	3.97584	−0.0396453	0.910490	1.08915
12	3.97583	−0.0396677	0.910383	1.09009
16	3.97583	−0.0396682	0.910379	1.09014
20	3.97583	−0.0396682	0.910379	1.09014

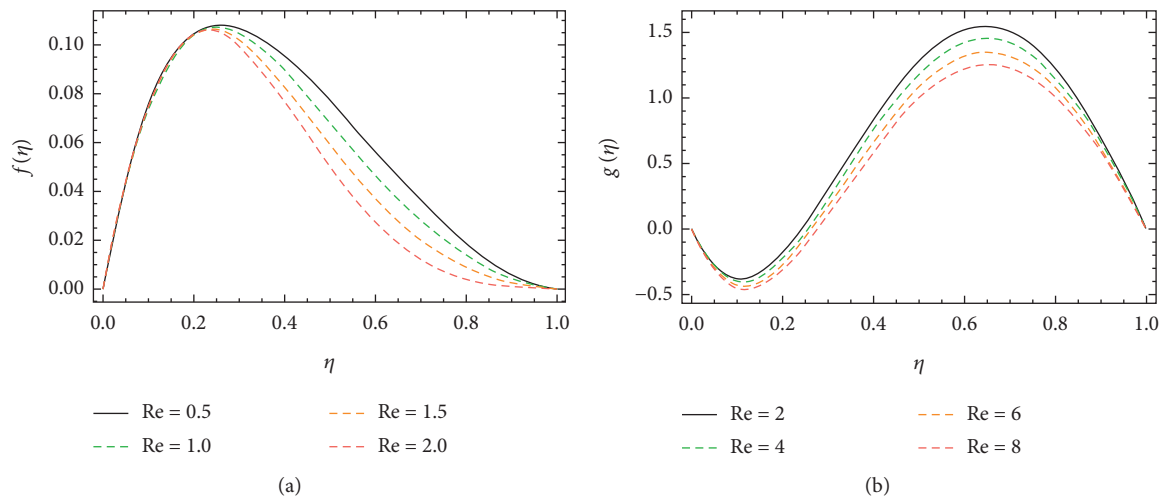

Figure 4: The influence of Re on $f(\eta)$ and $g(\eta)$ when $\gamma = 0.4, m = 0.7, \lambda_1 = 0.5, M = 1, \beta = 0.4, \mathrm{Kr} = 0.6$.

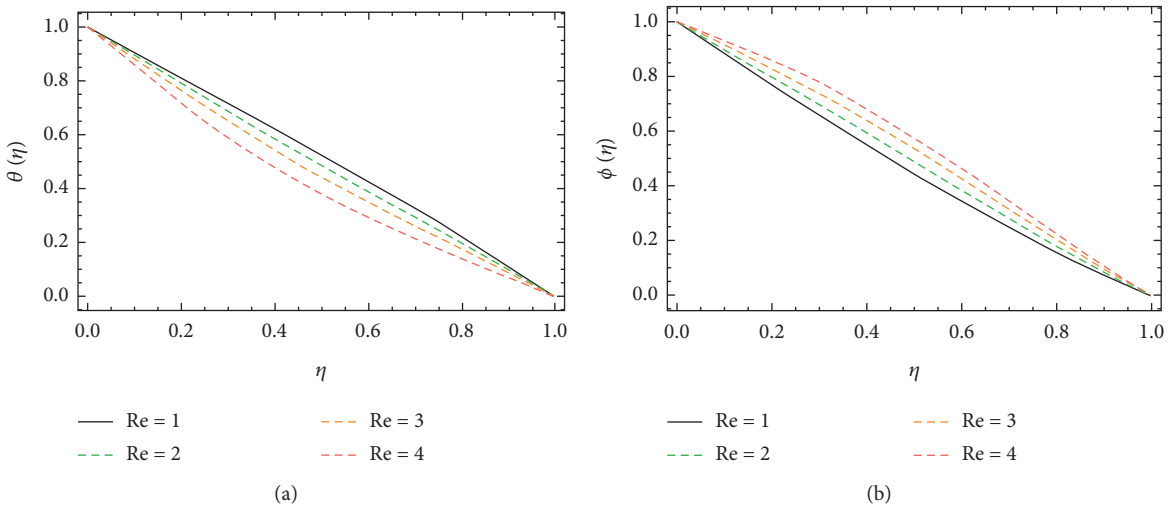

Figure 5: The influence of Reon $\Theta(\eta)$ and $\Phi(\eta)$ when $M = 1, \lambda_1 = m = 0.8, \beta = 0.4, \mathrm{Kr} = \gamma = 0.6, \mathrm{Nb} = \mathrm{Sc} = \mathrm{Nt} = \mathrm{Rd} = 0.5, \mathrm{Pr} = 5$.

along the y direction and greater value of Hall parameter m decrease the velocity profile along z direction. Figures 8(a) and 8(b) describe the effect of $\lambda_1$on velocity profiles $f(\eta)$ and $g(\eta)$. It displays that the rise in ratio of relaxation λ_1 decreases the relaxation time. The small values dominate the viscous forces. Actually, the rise in λ_1 shows viscoelastic effect, and as a result, the fluid motion is reduced. Figures 9(a) and 9(b) demonstrate the influence of the Deborah number on velocity distributions $f(\eta)$ and $g(\eta)$. The Deborah number β was first proposed by Markus Reiner; it is a dimensionless number, frequently used in fluid mechanics, to illustrate the flexibility of materials under definite flow situations. With the increase in Deborah number β, the velocity profile increases and has opposite effect to λ_1. The large relaxation time decreases the velocity field. The characteristics of Magnetic parameter M on

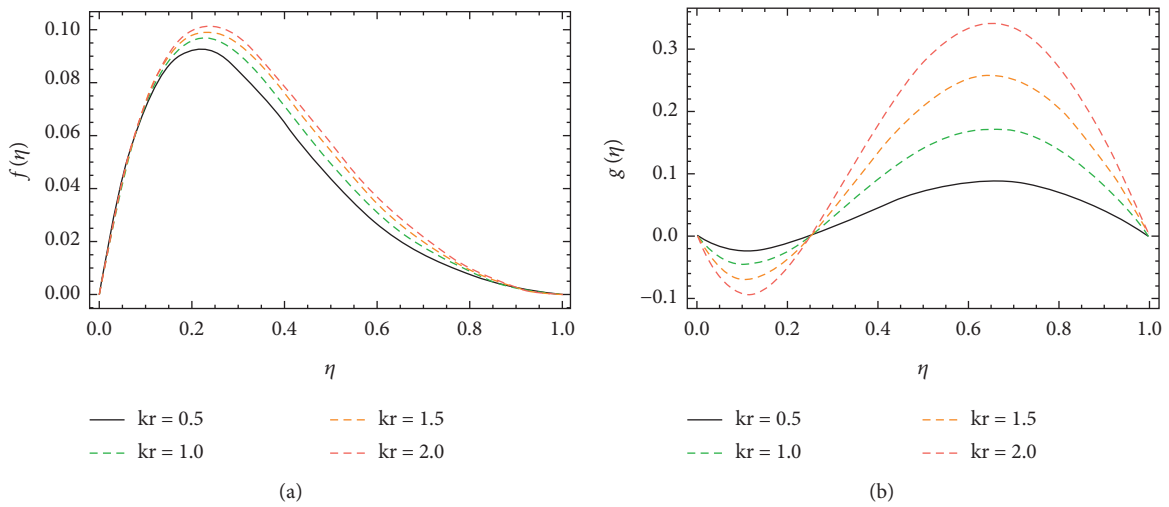

Figure 6: The influence of Kr on $f(\eta)$ and $g(\eta)$ when $m = \lambda_1 = 0.8, M = \beta = 1, \mathrm{Re} = 1, \gamma = 0.4$.

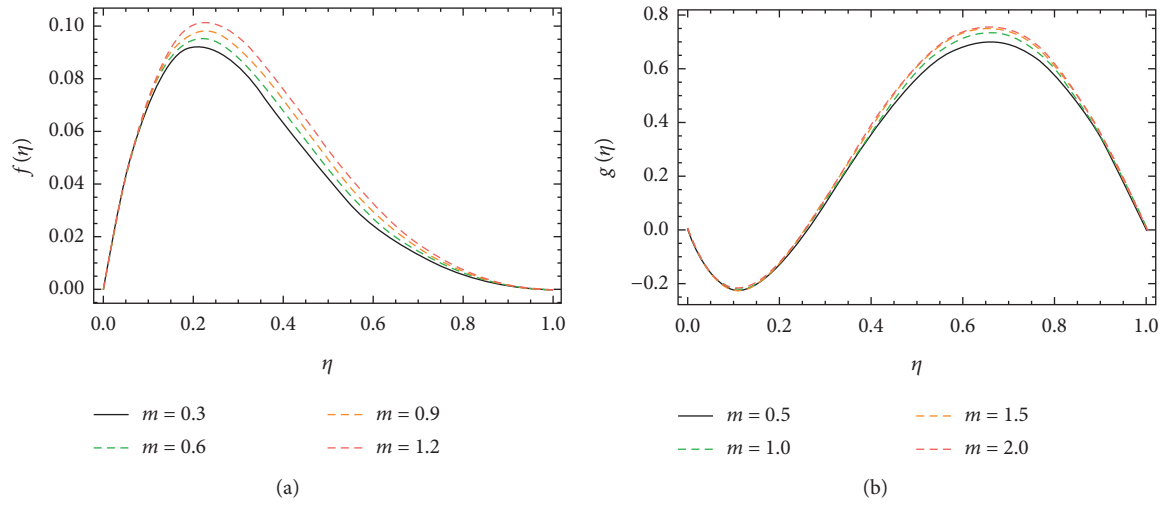

Figure 7: The influence of m on $f(\eta)$ and $g(\eta)$ when $\mathrm{Re} = 1, \lambda_1 = 0.8, M = \beta = 0.7, \mathrm{Kr} = 0.6, \gamma = 0.4$.

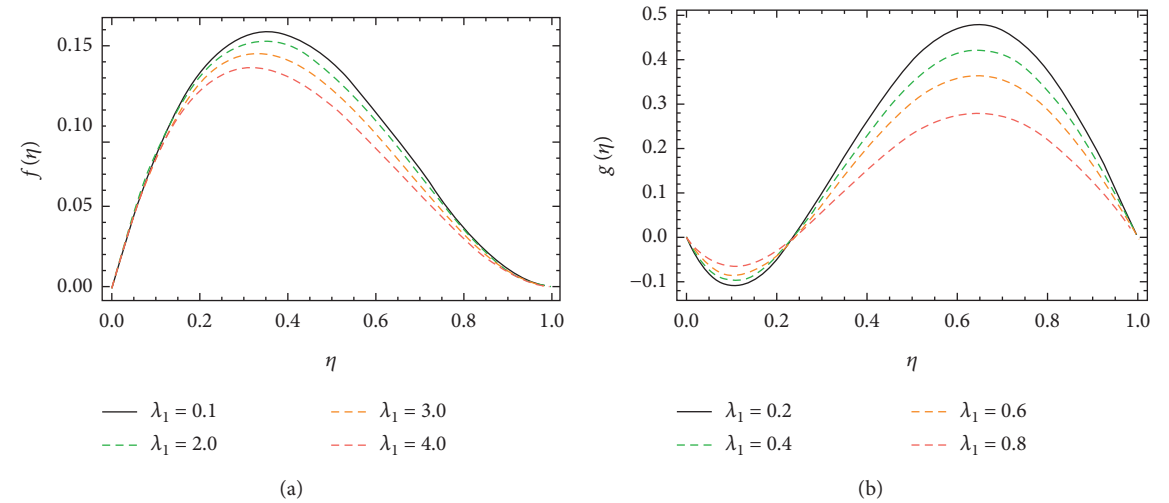

Figure 8: The influence of λ_1 on $f(\eta)$ and $g(\eta)$ when $\mathrm{Re} = 2, \beta = 0.8, M = 1.6, \gamma = 0.6, \mathrm{Kr} = 1.8, m = 0.7$.

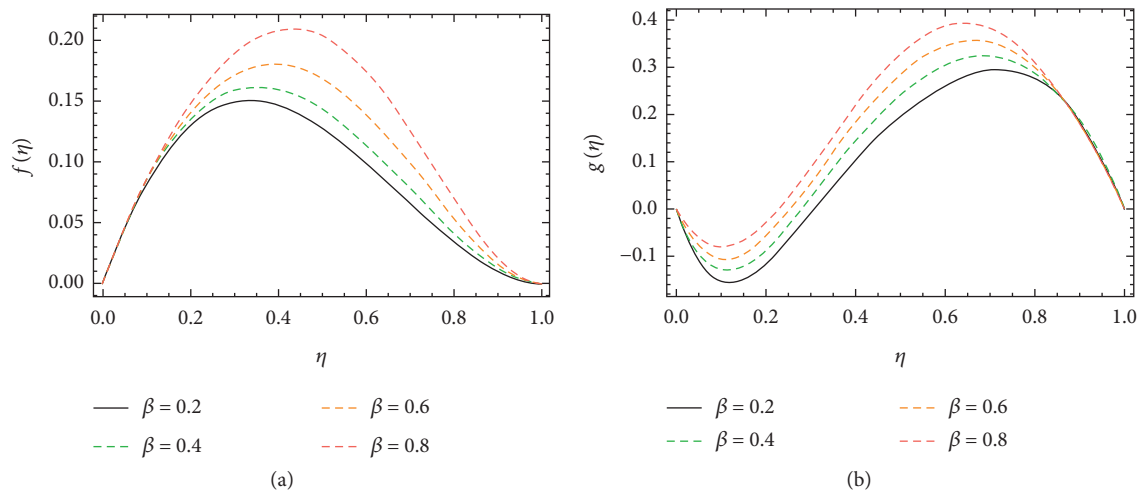

Figure 9: The influence of β on $f(\eta)$ and $g(\eta)$ when $\mathrm{Re} = 1, \lambda_1 = 0.7, M = 1, \gamma = 0.6, \mathrm{Kr} = m = 0.6$.

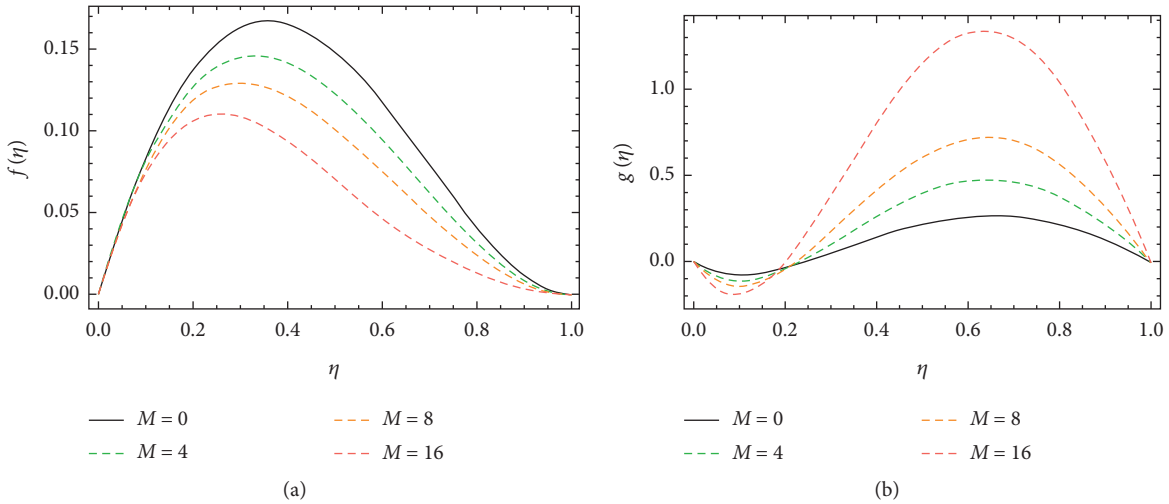

Figure 10: The influence of M on $f(\eta)$ and $g(\eta)$ when $\mathrm{Re} = 1, \lambda_1 = 0.8, M = \beta = 0.7, \mathrm{Kr} = \gamma = 0.6$.

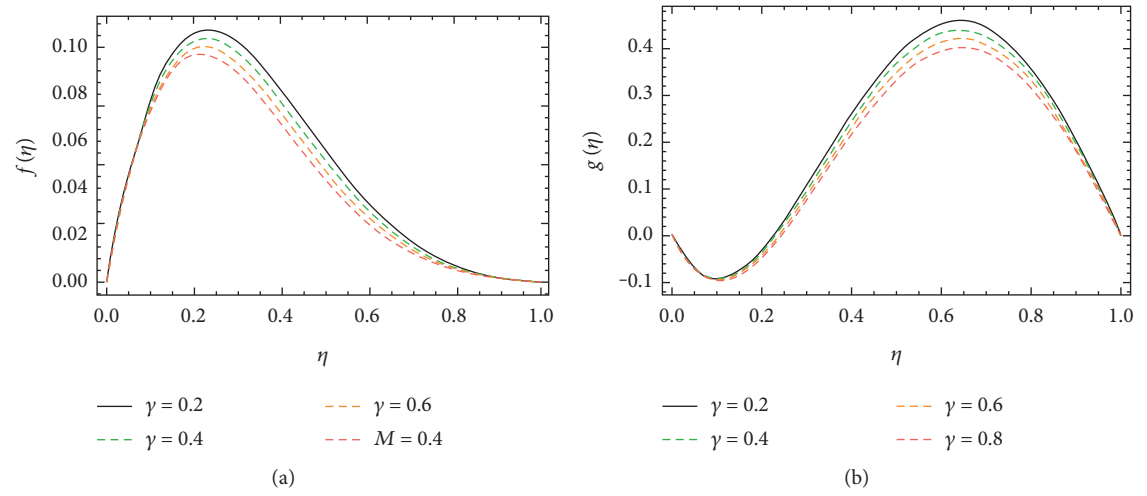

Figure 11: The influence of γ on $f(\eta)$ and $g(\eta)$ when $\mathrm{Re} = 1.5, \lambda_1 = 0.8, M = 1, \beta = 0.7, \mathrm{Kr} = m = 0.6$.

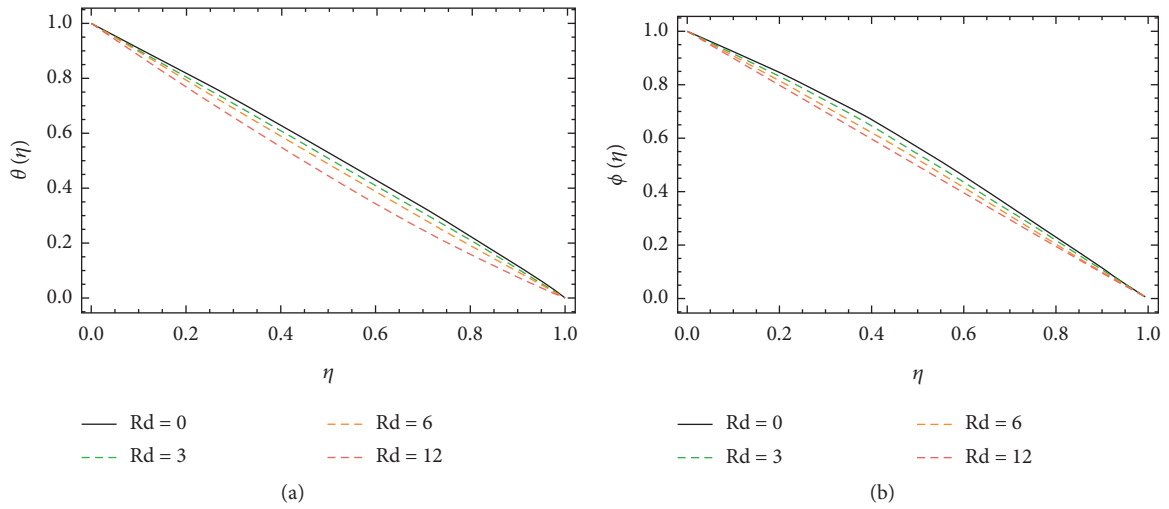

Figure 12: The influence Rd on $\Theta(\eta)$ and $\Phi(\eta)$ when $M = 1, \lambda_1 = m = 0.8, \beta = 0.4, \mathrm{Kr} = \gamma = 0.6, \mathrm{Nb} = \mathrm{Sc} = \mathrm{Nt} = \mathrm{Re} = 0.5, \mathrm{Pr} = 5$.

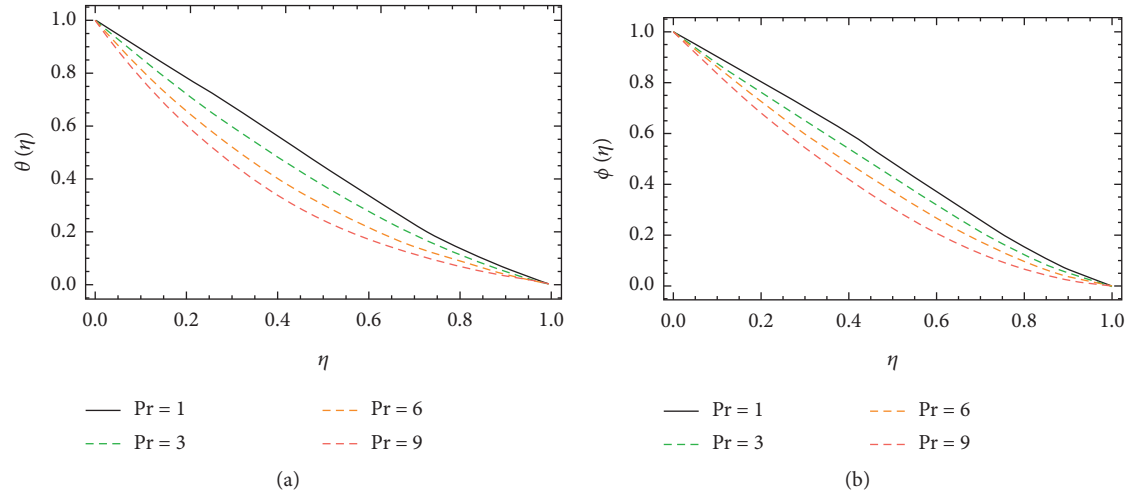

Figure 13: The influence of Pr on $\Theta(\eta)$ and $\Phi(\eta)$ when $M = 1, \lambda_1 = m = 0.8, \beta = 0.4, \mathrm{Kr} = 0.6, \mathrm{Nb} = \mathrm{Sc} = \mathrm{Nt} = \mathrm{Rd} = 0.5, \mathrm{Pr} = 5$.

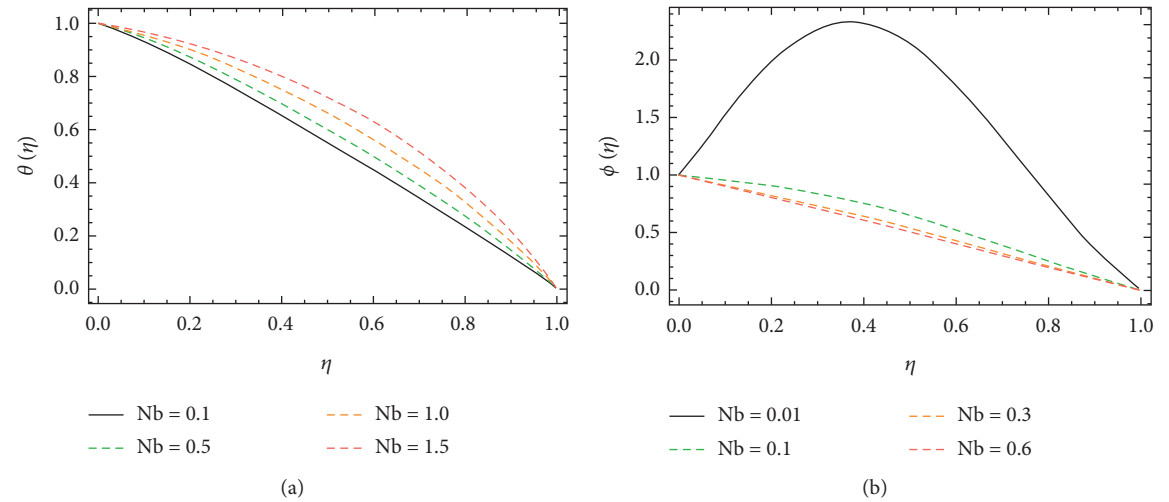

Figure 14: The influence Nb on $\Theta(\eta)$ and $\Phi(\eta)$ when $M = 1, \lambda_1 = m = 0.8, \beta = 0.4, \mathrm{Kr} = \gamma = 0.6, \mathrm{Re} = 1, \mathrm{Sc} = \mathrm{Nt} = 0.5, \mathrm{Rd} = 0.6, \mathrm{Pr} = 10$.

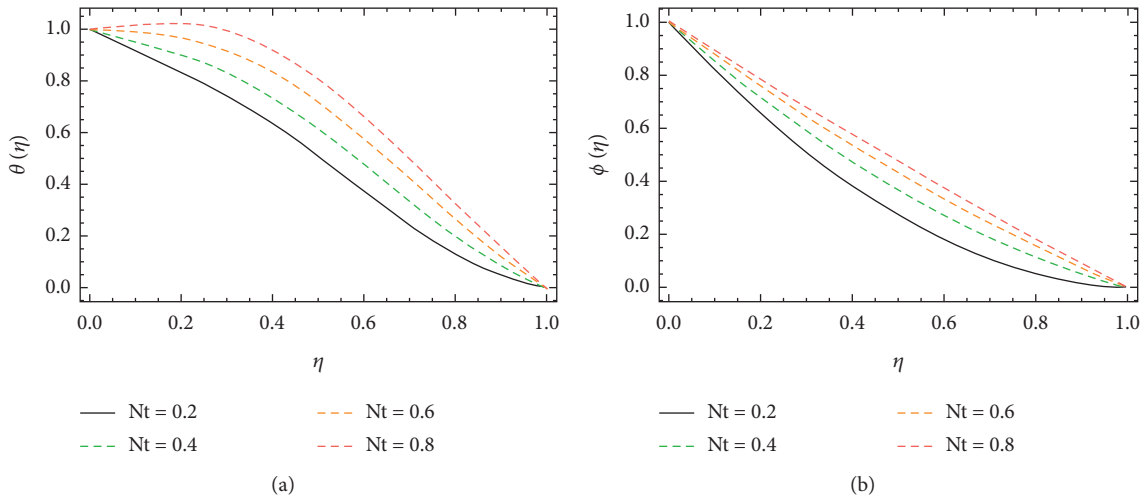

Figure 15: The influence Nb on $\Theta(\eta)$ and $\Phi(\eta)$ when $M = \gamma = \beta = 0.4, \lambda_1 = m = 0.8$, Sc = 0.5, Kr = 0.6, Re = 1, Nb = 0.2, Rd = 0.5, Pr = 1.

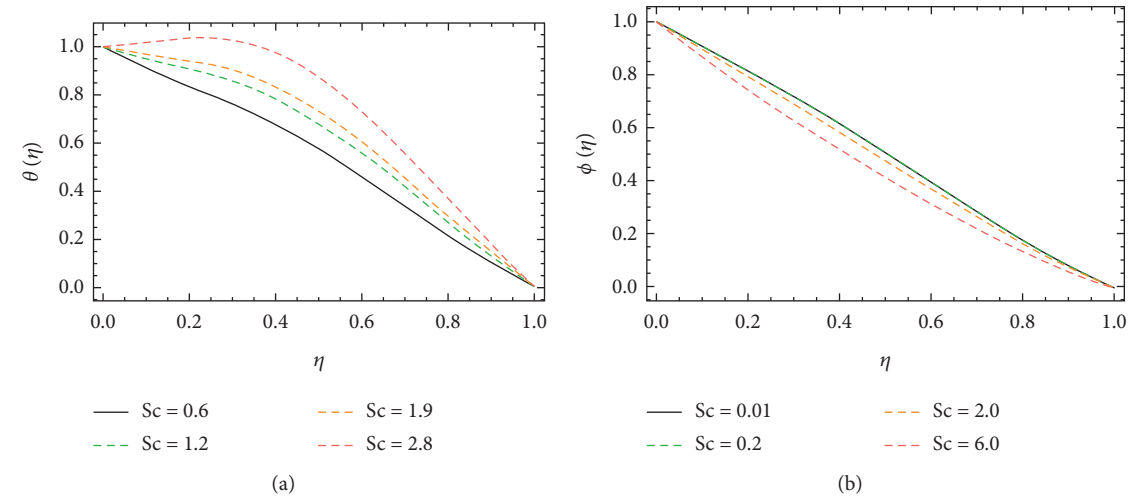

Figure 16: The influence Sc on $\Theta(\eta)$ and $\Phi(\eta)$ when $M = \gamma = \beta = 0.4, \lambda_1 = m = 0.8$, Kr = 0.6, Re = 1, 0.5, Nb = 0.4, Rd = 0.5, Pr = 1, Nt = 0.4.

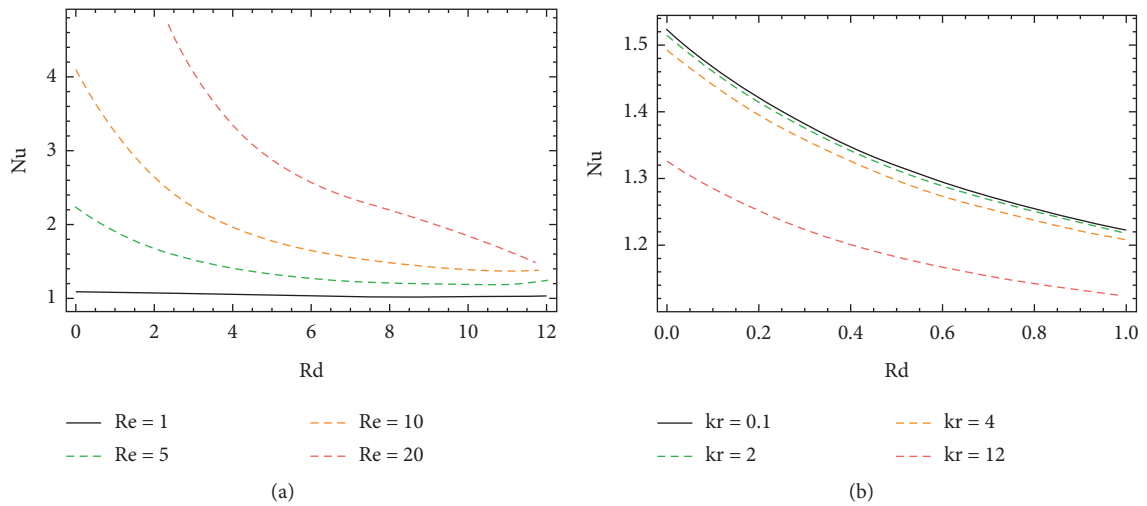

Figure 17: Continued.

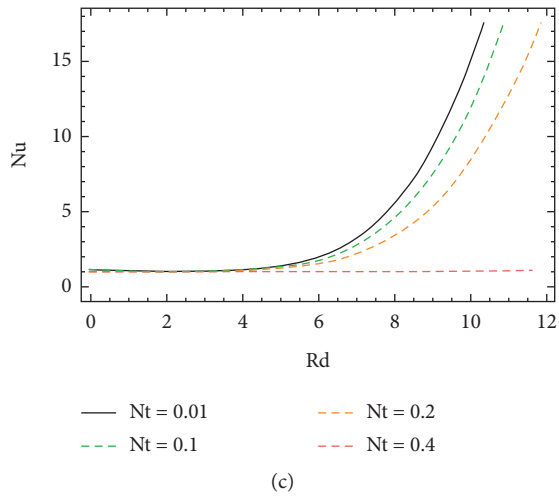

Figure 17: The influence Rd, Re, Nt and Kr on Nusselt numbers $(\mathrm{Nu} = -\Theta'(0))$ when $M = \gamma = \beta = 0.4, \lambda_1 = m = 0.8, \mathrm{Sc} = 1, \mathrm{Nb} = 0.3, \mathrm{Pr} = 1$, (a) $\mathrm{Kr} = 1, 0.5, \mathrm{Nt} = 0.01$. (b) $\mathrm{Re} = 1, \mathrm{Nt} = 0.01$. (c). $\mathrm{Kr} = 0.2, \mathrm{Re} = 1.0$.

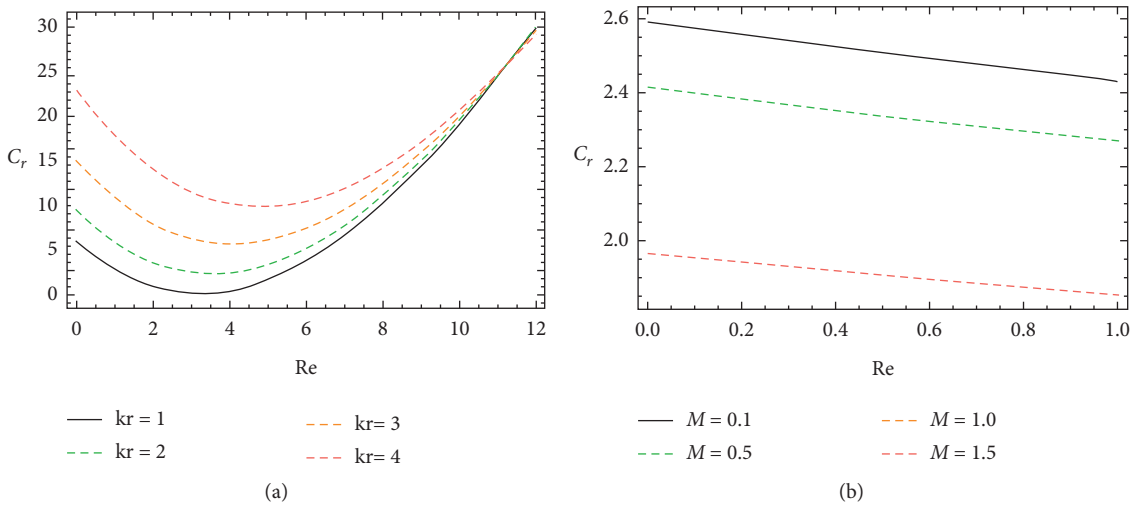

Figure 18: The influence of Kr, M and Kr on Skin friction C_f when $\beta = 0.4, \lambda_1 = m = 0.8$. (a) $\gamma = 0.1, M = 0.5$. (b). $\gamma = 0.1, \mathrm{Kr} = 0.6$.

velocity distributions have been shown in Figures 10(a) and 10(b) along y and z-directions, respectively. It is clear that the velocity distribution $f(\eta)$ is inversely varied with magnetic parameter M along the y direction and directly varied with $g(\eta)$ along the z-direction. Increasing magnetic parameter M decreases the velocity field along y direction, since the magnetic field is applied perpendicularly to y direction, and hence, the conducting fluid particles feel the opposite force of magnetic field and hence reduce the velocity profile along y direction as shown in Figure 10(a) when it is close to the plates. The effect of magnetic field along z direction is shown in Figure 10(b). The magnetic field is applied parallelly to z direction, and hence, it assists the flow. This is because of the fact that the rise in the M progresses the friction force of the movement, named the Lorentz force. Lorentz force has the affinity to reduce the velocity of the flow in the boundary sheet, where another force known as Coriolis force shows the reverse influence on the velocity along the z-direction. The characteristics of porosity parameter γ on velocity fields are shown in Figures 11(a) and 11(b) in y and z-directions, respectively, which have an imperative character in the flow motion. Increasing γ increases the porous space, which creates resistance in the flow path and reduces the flow motion. In fact, growing values of γ show the large number of porous spaces, which create resistance in the flow path and reduce overall fluid motion. Basically with the increase of the number of holes in the porous plate, the velocity decreases during the flow of nanofluid particles over these holes. The impact of thermal radiation parameter Rd on $\Theta(\eta)$ and $\Phi(\eta)$ is presented in Figures 12(a) and 12(b). The thermal radiation has an imperative role in the inclusive surface heat transmission when the coefficient of convection heat transmission is small. When we increase thermal radiation parameterRd, then it is perceived that it augments the temperature in the boundary layer area in the fluid layer.

This increase leads to a drop in the rate of cooling for nanofluid flow. The same effect is observed for the concentration distributions (Figure 12(b)). The influence of Pr on the temperature and concentration distributions $\Theta(\eta)$ and $\Phi(\eta)$ is shown in Figures 13(a) and 13(b). Both temperature and concentration distributions vary inversely with Pr. It is clear that temperature distribution decreases with large numbers of Pr and increases for small values of Pr. Physically, the fluids having a small number of Pr have larger thermal diffusivity, and this effect is opposite for higher Pr and tl number Pr. Due to this fact, large Pr causes the thermal boundary layer to decrease. The effect is even more distinct for the small number of Pr, since the thermal boundary layer thickness is relatively large. The same effect of Pr on concentration distribution is shown in Figure 13(b). Figures 14(a) and 14(b) show the features of Brownian motion parameter Nb on temperature distribution and concentration profile. Brownian motion is the inconsistent random motion of nanofluids particles. It has been initiated that the Brownian motion of nanoparticles at the molecular level is a central mechanism leading the thermal conductivity of nanofluids. The augmentation in the active thermal conductivity of nanofluids is due mostly to the contained convection produced by the Brownian movement of the nanoparticles. It is observed from Figure 14(a) that increasing Nb raises the temperature field. In fact, increasing Nb raises the kinetic energy of the nanoparticles inside the fluid, with which rate of heat transfer and boundary layer thickness rises, which leads to an increase in the temperature field. While the opposite impact has been found for concentration distribution that is increasing, the Nb reduces the concentration profile (Figure 14(b)). This is because the rise of Brownian motion diminishes the boundary layer thicknesses, which leads to reducing concentrations. The thermophoresis parameter Nt of temperature distribution and concentration field is shown in Figures 15(a) and 15(b). Thermophoresis is a process perceived in combinations of mobile particles of nanofluids, where the unlike particle kinds display different retorts to the force of a temperature gradient. It is observed from Figures 15(a) and 15(b) that Nt increases the temperature field when it increased, and the same effects of Nt are observed for concentration field. This is due to the thermophoresis parameter, and Nt depends on the temperature gradient in the surrounding nanofluids molecules. Increasing Nt increases the kinetic energy of the nanofluids molecules, which as a result increases the temperature and concentration profile. Figures 16(a) and 16(b) describe the effect of Schmidt number Sc, where Sc is a dimensionless number, and it is the ratio of momentum diffusivity and mass diffusivity. So, for large values of Sc, the temperature rises and falls for small values, while the opposite tendency is perceived in concentration field. Increasing Schmidt number decreases the concentration profile, which results in reducing the boundary layer thickness. Effect of viscosity parameter Ron Skin friction C_f against β and λ_1 is shown in Figures 17(a) and 17(b). There is inverse variation between skin friction and viscosity parameter; increasing R decreases the Skin friction C_f. Figure 17(c) demonstrates the effect of Kr on Skin friction C_f against β. It is observed that C_f increases with large values of rotation parameter Kr. Effect of R on Nusselt number Nu against Nt and Nb is shown in Figures 18(a) and 18(b) and it is found that, for large value of Nt and Nb, the mass flux increased Nu. This is because increasing Nt and Nb increases the kinetic energy of the nanofluids molecules, which as a result increases heat flux Nu. Figure 17 describes the effect of R on mass flux Sh against Nt, which shows that mass flux is increasing function when Nt increases.

5.2. Table Discussion. The effect of viscosity parameter Re and magnetic parameter M on Nusselt number and Sherwood number Sh is numerically shown in Tables 2 and 3. It is observed that both mass flux and heat flux are decreasing functions when the viscosity parameter Re and magnetic parameter M are increased. To validate our results, the obtained results are compared with the result available in the literature as given in Table 4. The influence of radiation parameter Rd and Schmidt number Sc on Nusselt number Nu and Sherwood numbers Sh is numerically shown in Tables 5 and 6. It is concluded that Nusselt number is reduced when the Schmidt number is increased, where, for radiation parameter, it shows opposite result. The obtained results are verified in comparison with the results of Sheikholeslami [17] given in Table 7 in order to validate our results. The effect of Nb and Nt on mass flux Nu and Sherwood numbers (heat flux) Sh is numerically shown in Tables 8 and 9. These tables show that increasing Nb and Nt increases the Nusselt number, where the opposite trend is found for Sherwood numbers Sh that the heat flux is decreased when Nb and Nt are increased. The obtained results are verified for validation in comparison with Sheikholeslami [17] results given in Table 10 which are in complete agreement with our results. The numerical values of $\mathrm{Re}, \lambda_1, \beta$ and kron skin friction C_f are given in Table 11. From this table, it is clear that increasing values of Re, λ_1 and β decreases C_f while increasing kr increases the skin friction. The numerical results (Table 11) and graphical result (Figures 14(a), 14(b), and 15) agree with each other. These results are compared with results of [19] given in Table 12. The obtained results are verified by comparing with [19] and good agreement is observed. The numerical values of heat flux Nu and mass flux Share given in Table 13. We have calculated it at the boundaries of the plates for dissimilar values of Nt, Nb and Sc. It is clear from Table 13 that the heat flux Nu is reduced when parameters Nt and Nb rose, because the mass flux is a reducing function of the lower stretching plate, where it is an growing function of Sc at the upper plate. The mass flux Sh is increasing function at the lower stretching plate, while it is a decreasing function of the upper plate at different increasing values of Nt, Nb and Sc. To validate and verify our results, the obtained results are compared with the RK Method of order 4 as given in Tables 14 and 15 , while the absolute errors of these methods are presented in Table 16 at each point.

Table 2: Influence of Rd and M on nusselt number Nu (present results), when Nt = Nb = 0.01, $R = 1, \beta = \gamma = 0.1$, Sc = 0.5, Pr = 10, $\lambda_1 = m = M = 0.01$.

Rd	M			
	0.0	4.0	8.0	16.0
0.0	1.42994	1.39765	1.36802	1.31676
3.0	1.65834	1.64590	1.55613	1.36460
6.0	3.19243	3.12424	3.09415	3.06673
12.0	12.1881	12.0005	11.9107	11.8235

Table 3: Influence of Rd and M on sherwood number Sh, when Nt = Nb = 0.01, $R = 1, \beta = \gamma = 0.1$, Sc = 0.5, Pr = 10, $\lambda_1 = m = M = 0.01$.

Rd	M			
	0.0	4.0	8.0	16.0
0.0	0.999128	0.998351	0.997707	0.996820
3.0	1.02138	1.02060	1.01996	1.01907
6.0	1.04363	1.04285	1.04221	1.04132
12.0	1.08813	1.08735	1.08671	1.08582

Table 4: Influence of Rd and M on nusselt number Nu (Sheikholeslami [17]), when Nt = Nb = 0.01, $R = 1$, Sc = 0.5, Pr = 10.

Rd	M			
	0.0	4.0	8.0	16.0
0.0	1.557044	1.523667	1.4954	1.449936
3.0	6.830242	6.802148	6.778303	6.739817
6.0	12.1581	12.13053	12.10713	12.06931
12.0	17.48938	17.46202	17.43877	17.40121

Table 5: Influence of Rd and Sc on nusselt number Nu (present results) when Nt = Nb = 0.01, $R = 1, \beta = \gamma = 0.1$, Sc = 0.5, Pr = 10, $\lambda_1 = m = M = 0.01$.

Rd	Sc			
	0.01	0.2	2.0	6.0
0.0	1.44402	1.44401	1.38730	1.38722
3.0	1.47528	1.38812	1.38684	1.38282
6.0	3.29221	3.27156	3.27150	3.27112
12.0	12.9804	12.9150	12.9002	12.8157

Table 6: Influence of Rd and Scon sherwood number Sh, when Nt = Nb = 0.01, $R = 1, \beta = \gamma = 0.1$, Sc = 0.5, Pr = 10, $\lambda_1 = m = M = 0.01$.

Rd	Sc			
	0.01	0.2	2.0	6.0
0.0	0.751084	0.758817	0.832441	1.01687
3.0	0.898084	1.00382	1.07744	1.26187
6.0	1.24108	1.04285	1.32244	1.50687
12.0	1.73108	1.73367	1.81244	1.99687

Table 7: Influence of Rd and Sc on nusselt numbers Nu (Sheikholeslami [17]), Nt = Nb = 0.01, $R = 1$, Sc = 0.5, Pr = 10.

Rd	Sc			
	0.01	0.2	2.0	6.0
0.0	1.557044	1.557021	1.556798	1.556285
3.0	6.830242	6.830225	6.830065	6.829702
6.0	12.1581	12.25808	12.15792	12.15757
12.0	17.48938	17.48936	17.48921	17.48886

Table 8: Influence of Rd and Nb on nusselt number Nu (present results), when Nt = Nb = 0.01, $R = 1, \beta = \gamma = 0.1$, Sc = 0.5, Pr = 10, $\lambda_1 = m = M = 0.01$.

Rd	Nb			
	0.01	0.1	0.3	0.6
0.0	1.46813	1.42162	1.32067	1.17551
3.0	1.38985	1.35748	1.28312	1.16532
6.0	3.27157	3.07334	2.62556	1.93514
12.0	12.915	11.8451	9.45044	5.81478

Table 9: Influence of Rd and schmidt number Sc on sherwood number Sh when Nt = Nb = 0.01, $R = 1, \beta = \gamma = 0.1$, Sc = 0.5, Pr = 10, $\lambda_1 = m = M = 0.01$.

Rd	Nb			
	0.01	0.1	0.3	0.6
0.0	0.766615	0.998921	1.01611	1.02038
3.0	1.01161	1.02117	1.02186	1.022
6.0	1.25661	1.04342	1.02761	1.02363
12.0	1.74661	1.08792	1.03911	1.02688

Table 10: Influence of Rd and Nb on nusselt number Nu (Sheikholeslami [17]), Nt = Nb = 0.01, $R = 1$, Sc = 0.5, Pr = 10.

Rd	Nb			
	0.01	0.1	0.3	0.6
0.0	1.557044	1.49911	1.37463	1.199351
3.0	6.830242	6.783053	6.678947	6.524752
6.0	12.1581	12.119	12.00966	12.85736
12.0	17.48938	17.44356	17.34201	17.19043

Table 11: The skin friction coefficient for dissimilar values of Re, Kr, β, and γ whenNt = Nb = 0.1, Sc = 0.5, Pr = 10, $\lambda_1 = m = M = 0.3$.

Re	M	γ	Kr	$-(C_f \mathrm{Re}_x)^{(1/2)}$
0.1	0.5	1.0	1.5	3.33027
0.5				2.94882
1.0				2.64208
1.5	0.1			4.33999
	0.5			4.32157
	1.0			4.26897
	1.5	0.1		5.64227
		0.5		5.44576
		1.0		4.89911
		1.5	0.1	4.12743
			0.5	4.35772
			1.0	5.13048
			1.5	5.91612

Table 12: Variation in skin friction coefficient for dissimilar values of Sq, ω, β, and λ_1 when Pr = 1.0, $\gamma = 1.0$ ([19] results).

sq	ω	λ_1	β	$-(C_f \mathrm{Re}_x)^{(1/2)}$
−0.1	0.5	1.0	0.5	2.63312
0.0				2.65133
0.1				2.63995
1.0	0.0			1.31217
	0.1			1.25917
	0.5			1.21694
	1.0	0.0		2.38508
		0.1		1.25917
		0.5		1.03399
		1.0	0.0	0.61911
			0.01	0.79884
			0.1	0.87732
			0.2	2.63312

Table 13: The effect of physical parameters on nusselt numbers Nu and sherwood number Sh when Nt = kr = 0.1, $R = 0.5$, Pr = 10, $\lambda_1 = m = M = 0.3$.

Rd	Nb	Sc	$\eta = +1$		$\eta = -1$	
			Nu	Sh	Nu	Sh
0.1	0.5	0.5	−0.766570	−1.70054	0.76657	1.70054
0.5			−0.622278	−1.23328	0.622278	1.23328
1.0			−0.459501	−1.17253	0.459501	1.17253
1.5	0.1		−0.414644	−1.02677	0.414644	1.02677
	0.5		−0.316268	−1.15054	0.316268	1.15054
	1.0		−0.215401	−1.35636	0.215401	1.35636
	1.5	0.1	−0.135599	−1.60728	0.135599	1.60728
		0.5	−0.135444	−1.60922	0.135444	1.60922
		1.0	−0.1353148	−1.61922	0.135251	1.61165
		1.5	−0.135057	−1.61408	0.135057	1.61408

Table 14: Results obtained by HAM at 20th order approximations when Rd = 0.5, Re = Nt = Nb = β = Sc = Pr = $\lambda_1 = M = m == 0.1, M = 1, \gamma = 0.5$.

η	$f(\eta)$	$g(\eta)$	$\Theta(\eta)$	$\Phi(\eta)$
0	0.00000	0.00000	1.00000	1.00000
0.1	1.32558	1.23456	0.987546	0.987542
0.2	1.23456	1.23546	0.845763	0.844587
0.3	2.34560	2.54686	0.745263	0.742145
0.4	2.45876	2.54896	0.675468	0.674578
0.5	2.62548	2.75625	0.564863	0.564578
0.6	2.32456	2.45236	0.420635	0.422214
0.7	2.01245	2.24563	0.321487	0.301245
0.8	1.56235	1.23555	0.214587	0.201245
0.9	1.254863	1.21452	0.11423	0.101123
1.0	0.000000	0.000000	0.00000	0.00000

Table 15: RK method of order 4, when Rd = 0.5, Re = Nt = Nb = β = Sc = Pr = $\lambda_1 = M = m == 0.1, M = 1, \gamma = 0.5$.

η	$f(\eta)$	$g(\eta)$	$\Theta(\eta)$	$\Phi(\eta)$
0	0.00000	0.00000	1.00000	1.00000
0.1	1.32558	1.23456	0.987546	0.987542
0.2	1.23456	1.23546	0.845763	0.844587
0.3	2.34560	2.54686	0.745263	0.742145
0.4	2.45876	2.54896	0.675468	0.674578
0.5	2.62548	2.75625	0.564863	0.564578
0.6	2.32456	2.45236	0.420635	0.422214
0.7	2.01245	2.24563	0.321487	0.301245
0.8	1.56235	1.23555	0.214587	0.201245
0.9	1.254863	1.21452	0.11423	0.101123
1.0	0.000000	0.000000	0.00000	0.00000

Table 16: Absolute errors of RK method of order 4 and HAM results when Rd = 0.5, Re = Nt = Nb = β = Sc = Pr = $\lambda_1 = M = m == 0.1, M = 1, \gamma = 0.5$.

η	$f(\eta)$	$g(\eta)$	$\Theta(\eta)$	$\Phi(\eta)$
0	0.00000	0.00000	0.00000	0.00000
0.1	1.22213×10^{-9}	1.32145×10^{-8}	2.14785×10^{-7}	1.65478×10^{-7}
0.2	2.13456×10^{-10}	3.214560×10^{-9}	2.85632×10^{-8}	1.25463×10^{-8}
0.3	2.14589×10^{-11}	1.32456×10^{-10}	2.45782×10^{-9}	1.87546×10^{-9}
0.4	1.54879×10^{-11}	2.001245×10^{-10}	1.24586×10^{-10}	1.85457×10^{-10}
0.5	2.14578×10^{-12}	1.02145×10^{-11}	3.12458×10^{-11}	1.24586×10^{-11}
0.6	2.145892×10^{-13}	1.02145×10^{-12}	5.45786×10^{-13}	1.45876×10^{-13}
0.7	2.45866×10^{-14}	1.021456×10^{-12}	3.54689×10^{-15}	1.45826×10^{-15}
0.8	2.001458×10^{-15}	1.02145×10^{-13}	2.47896×10^{-16}	1.85475×10^{-16}
0.9	2.14586×10^{-18}	2.14586×10^{-17}	1.24589×10^{-17}	1.98526×10^{-17}
1.0	0.000000	0.000000	0.000000	0.000000

6. Conclusion

The present study explores the magnetohydromagnetic flow of Jeffrey nanofluid between two parallel plates with Hall current effect. The governing equations are transformed to obtain a set of nonlinear ODEs. The optimal solution is obtained by HAM, while the numerical solution is obtained by RK Method of order 4. The observation of this work depends on the influence of Hall current, porosity, and rotation of non-Newtonian nanofluid flow between two parallel plates. The mathematical formulation of the model has been carried out in such a manner that one of the plates is stretched, and the other is fixed. The constant magnetic field is considered, and it is acting perpendicularly to the direction of the flow field. The modeled equations have been solved through analytical homotopy analysis method HAM. The convergence of the HAM method has been shown numerically. Also, the system of equation is solved numerically by RK Method of order 4 for validating the obtained results. The effect of the embedded parameter is observed and studied graphically. The influence of skin friction C_f is shown graphically as well as numerically, and also its effects on different parameter like β, λ_1, M and kr are observed graphically and numerically. The influence of the Nuslet number Nu and the Sherwood number Sh on the temperature and concentration fields has been observed. The central concluded key points are as follows:

(i) The larger values of Brownian motion parameter Nb raise the kinetic energy of the nanoparticles inside the fluid, and as a result, the profile of the temperature rises.

(ii) Thermal boundary layer thickness reduces with the rise of radiation parameter Rd. So, Nusselt number Nu rises with rise of radiation parameter Rd.

(iii) The higher values of the Hall parameter$m$ increase the velocity of the nanofluid because Hall force transfers forward the nanoliquids in horizontal direction.

(iv) For skin friction C_f it is found that it is increased when the viscosity parameter Re is decreased.

(v) The mass flux has been observed as a decreasing function at the lower stretching plate and an increasing function of Sc at the upper static plate.

(vi) The heat flux Sh has been concluded as an increasing function at the lower stretching plate and decreasing function at upper static plate.

(vii) HAM is fastly convergent when compared to other methods.

(viii) The absolute errors decrease by increasing η.

Nomenclature

a,b,c: Constants
$\widetilde{B}$: Magnetic field (NmA^{-1})
C: Fluid concentration
c_p: Specific heat (J/kgK)
C_f: Skin friction coefficient
D_B: Brownian diffusion of nanofluids
D_T: Thermophoretic diffusion of nanofluids
$\widetilde{E}$: Electric field intensity (NC^{-1})
$\widehat{F}_1, \widehat{F}_2$: Homotopic functions
h: Distance between the plates
J_w: Mass flux
k: Thermal conductivity ($\mathrm{Wm}^{-1}\mathrm{K}^{-1}$)
Kr: Rotation parameter
k: The boundary parameter
M: Magnetic parameter
m: Hall parameter
n_e: Number density of electron
Nb: Brownian motion
Nt: Thermophoretic parameter
Nu: Nusselt number
O: Origen
P: Fluid pressure (Pa)
Pr: Prandtl number
Q_w: Heat flux (Wm^{-2})
q_r: Radioactive heat flux (J)
Re: Viscosity parameter
Rd: Radiation parameter
R_{ex}: Local Reynolds number
S: Cauchy stress tensor
Sc: Schmidt number
Sh: Sherwood number
t_e: Flow time (s)
T: Fluid temperature (K)
u, v w: Velocities components (ms^{-1})
u_w: Stretching velocity (ms^{-1})
x, y, z: Coordinates
X,Y: Topological space.

Greek Letters

α: Thermal diffusivity ($\mathrm{m}^2\mathrm{s}^{-1}$)
η: Similarity variable.
$\widehat{\kappa}$: Vertex viscosity (mPa)
κ_m: Constants where $m = 1, 2, \ldots$
μ: Dynamic viscosity (mPa)
υ: Kinematic coefficient of viscosity
ρ_f: Base fluid density (Kgm^{-3})
ρ_b: Density of the particles (Kgm^{-3})
σ_{nf}: Electrical conductivity of nanofluid (Sm^{-1})
τ^*: Ratio of nanoparticles and heat capacity
φ: Stefan Boltzmann constant
h: Assisting parameter
Φ: Dimensional concentration profile
ω_e: Oscillating frequency of the electron (S^{-1})
Ω: Angular velocity (ms^{-1}).

Data Availability

All the relevant data are available in the paper. However, more can be provided on request if someone needs it.

Conflicts of Interest

The authors declare that they have no conflicts of interest.

References

[1] S. U. S. Choi and J. A. Estman, "Enhancing thermal conductivity of fluids with nanoparticles," *ASME-Publications-Fed*, vol. 231, pp. 99–106, 1995.

[2] T. Hayat, K. Muhammad, M. Farooq, and A. Alsaedi, "Squeezed flow subject to Cattaneo-Christov heat flux and rotating frame," *Journal of Molecular Liquids*, vol. 220, pp. 216–222, 2016.

[3] T. Hayat, M. Waqas, and A. Alsaedi, "MHD stagnation point flow of Jeffrey fluid by a radially stretching surface with viscous dissipation and Joule heating," *Journal of Hydrology and Hydromechanics*, vol. 63, no. 4, pp. 311–317, 2015.

[4] H. Alfvén, "Existence of electromagnetic-hydrodynamic waves," *Nature*, vol. 150, no. 3805, pp. 405-406, 1942.

[5] M. Umeshaiah, B. C. Prasannakumara, and M. Archana, "Impact of nonlinear thermal radiation on magnetohydrodynamic three dimensional boundary layer flow of Jeffrey nanofluid over a nonlinearly permeable stretching sheet," *Physica A: Statistical Mechanics and Its Applications*, vol. 549, Article ID 124051, 2020.

[6] E. H. Hall, "On a new action of the magnet on electric currents," *American Journal of Mathematics*, vol. 2, no. 3, pp. 287–292, 1879.

[7] I. Pop and V. M. Soundalgekar, "Effects of Hall current on hydromagnetic flow near a porous plate," *Acta Mechanica*, vol. 20, no. 3-4, pp. 315–318, 1974.

[8] S. Ahmed and J. Zueco, "Modeling of heat and mass transfer in a rotating vertical porous channel with hall current," *Chemical Engineering Communications*, vol. 198, no. 10, pp. 1294–1308, 2011.

[9] M. Abdel Aziz, "Effects of hall current on the flow and heat transfer of a nanofluid over a stretching sheet with partial slip," *International Journal of Modern Physics C*, vol. 24, no. 7, Article ID 1350044, 2013.

[10] T. Hayat, M. Awais, M. Nawaz, S. Iram, and A. Alsaedi, "Mixed convection three-dimensional flow with Hall and ion-slip effects," *International Journal of Nonlinear Sciences and Numerical Simulation*, vol. 14, no. 3–4, pp. 167–177, 2013.

[11] P. Sulochana, "Hall effects on unsteady mhd three dimensional flow through a porous medium in a rotating parallel plate channel with effect of inclined magnetic field," *American Journal of Computational Mathematics*, vol. 04, no. 05, pp. 396–405, 2014.

[12] K. Das, U. S. S. Sarit, and Y. U. Choi, *Wenhua, Pradeep, Nanofluids,Science and Technology*, Wiley-Interscience, Hoboken, NJ, USA, 2007.

[13] X.-Q. Wang and A. S. Mujumdar, "A review on nanofluids - part II: experiments and applications," *Brazilian Journal of Chemical Engineering*, vol. 25, no. 4, pp. 631–648, 2008.

[14] S. Goodman, "Radiant-heat transfer between nongray parallel plates," *Journal of Research of the National Institute of Standards*, vol. 58, p. 2732, 1957.

[15] A. K. Borkakoti and A. Bharali, "Hydromagnetic flow and heat transfer between two horizontal plates, the lower plate being a stretching sheet," *Quarterly of Applied Mathematics*, vol. 40, no. 4, pp. 461–467, 1983.

[16] H. A. Attia, N. A. Kotb, and C. Egypt, "MHD flow between two parallel plates with heat transfer," *Acta Mechanica*, vol. 117, no. 1–4, pp. 215–220, 1996.

[17] M. Sheikholeslami and D. D. Ganji, "Three dimensional heat and mass transfer in a rotating system using nanofluid," *Powder Technology*, vol. 253, pp. 789–796, 2014.

[18] M. Mahmoodi and S. Kandelousi, "Kerosene–alumina nanofluid flow and heat transfer for cooling application," *Journal of Central South University*, vol. 23, no. 4, pp. 983–990, 2016.

[19] M. S. Tauseef, Z. Ali, K. Z. Khan, and N. Ahmed, "On heat and mass transfer analysis for the flow of a nanofluid between rotating parallel plates," *Aerospace Science and Technology*, vol. S1270-9638, pp. 00227-00228, 2015.

[20] H. B. Rokni, D. M. Alsaad, and P. Valipour, "Electro-hydrodynamic nanofluid flow and heat transfer between two plates," *Journal of Molecular Liquids*, vol. 216, pp. 583–589, 2016.

[21] M. Fiza, H. Ullah, and S. Islam, "Three dimensional MHD rotating flow of viscoelastic nanofluid in porous medium between two parallel plates," *Journal of Porous Media*, vol. 23, pp. 715–729, 2014.

[22] G. S. Taylor, "Experiments with rotating fluids," *Proceedings of the Royal Society of London*, vol. 100, pp. 114–121, 1921.

[23] H. P. Greenspan, "The theory of rotating fluid," *Journal of Fluid Mechanics*, vol. 52, pp. 794–797, 1972.

[24] K. Vajravelua and B. V. R. Kumar, "Analytical and numerical solutions of a coupled non-linear systemarising in a three-dimensional rotating flow," *International Journal of Non-linear Mechanics*, vol. 39, pp. 13–24, 2004.

[25] A. Mehmood and A. Ali, "Analytic solution of three-dimensional viscous flow and heat transfer over a stretching flat surface by homotopy analysis method," *Journal of Heat Transfer*, vol. 13, pp. 121701–121704, 2008.

[26] T. Hayat, S. Qayyum, M. Imtiaz, and A. M. Alsaedi, "Three-dimensional rotating flow of jeffrey fluid for cattaneo-christov heat flux model," *AIP Advances*, vol. 6, Article ID 025012, 2016.

[27] S. Nadeem, M. Sadaf, M. Rashid, and M. S. Adil, "Optimal and numerical solutions for an MHD micropolar nanofluid between rotating horizontal parallel plates," *PLoS One*, vol. 10, no. 6, Article ID e0124016, 2015.

[28] M. Jena, M. Goswami, and S. Biswal, "Heat and mass transfer in the MHD flow of a visco-elastic fluid in a rotating porous channel with radiative heat," *Proceedings of the National Academy of Sciences*, vol. 84, pp. 527–534, 2014.

[29] G. B. Jeffrey, "The motion of ellipsoidal particles immersed in a viscous fluid," *Proceedings of the Royal Society of London*, vol. 102, pp. 161–179, 1922.

[30] A. Shehzad, A. Hayat, and A. Alsaedi, "MHD flow of Jeffrey nanofluid with convective boundary conditions," *Journal of the Brazilian Society of Mechanical*, vol. 37, 2014.

[31] T. Hayat, T. Muhammad, S. A. Shehzad, and A. Alsaedi, "Three-dimensional flow of jeffrey nanofluid with a new mass flux condition," *Journal of Aerospace Engineering*, vol. 56, 2015.

[32] A. B. Kumari, K. Ramakrishna, and K. Kavitha, "Effects of a magnetic field on the free convective flow of jeffrey fluid past an infinite vertical porous plate with constant heat flux," *International Journal of Mathematical Archive*, vol. 3, no. 6, pp. 2240–2248, 2012.

[33] A. A. Farooq, B.. Belal, and A. M. Siddiqui, "Lifting of a Jeffrey fluid on a vertical belt under the simultaneous effects of magnetic field and wall slip conditions," *International Journal of Advanced Mathematical, Sciences*, vol. 1, no. 2, pp. 91–97, 2013.

[34] A. Naveed, K. Umar, and S. M. Tauseef, "Two-dimensional flow of a Jeffery fluid in a dilating and squeezing porous channel," *World Journal of Modelling and Simulation*, vol. 12, no. 1, pp. 59–69, 2016.

[35] K. Asadullah, A. Naveed, M. Raheela, and S. M. D. Tauseef, "MHD Flow of a Jeffery fluid in converging and diverging channels," *International Journal of Modern Mathematical Sciences*, vol. 6, no. 2, pp. 92–106, 2013.

[36] A. Zeeshan and A. Majeed, "Heat transfer analysis of Jeffery fluid flow over a stretching sheet with suction/injection and magnetic dipole effect," *Alexendria Engineering Journal*, vol. 55, no. 3, pp. 2171–2181, 2013.

[37] A. Riaz, S. Nadeem, R. Ellahi, and A. Zeeshan, "Exact solution for peristaltic flow of Jeffrey fluid model in a three dimensional rectangular duct having slip at the walls," *Applied Bionics and Biomechanics*, vol. 11, no. 1, pp. 81–90, 2012.

[38] S. J. Liao, *The proposed homotopy analysis method for the solution of nonlinear problems*, PhD Thesis, Shangai Jiao Tong Universit, Shanghai, China, 1992.

[39] S. J. Liao, "An analytic solution of unsteady boundary layer flows caused by impulsively stretching plate," *Communications in Nonlinear Science and Numerical*, vol. 11, pp. 326–339, 2004.

[40] S. J. Liao, "An optimal homotopy-analysis approach for strongly nonlinear differential equations," *Communications in Nonlinear Science and Numerical Simulation*, vol. 15, pp. 2003–2016, 2010.

[41] Z. Shah, T. Gulb, S. Islama et al., "Three dimensional third grade nanofluid flow in a rotating system between parallel plates with Brownian motion and thermophoresis effects," *Results in Physics*, vol. 10, pp. 36–45, 2018.